JOURNAL OF GEOPHYSICAL RESEARCH, VOL. 115, B06401, doi:10.1029/2009JB006896, 2010

A model for the evolution of the Earth's mantle structure since the Early Paleozoic

Nan Zhang,[1] Shijie Zhong,[1] Wei Leng,[1] and Zheng-Xiang Li[2]

Received 20 August 2009; revised 27 December 2009; accepted 14 January 2010; published 4 June 2010.

[1] Seismic tomography studies indicate that the Earth's mantle structure is characterized by African and Pacific seismically slow velocity anomalies (i.e., superplumes) and circum-Pacific seismically fast anomalies (i.e., a globally spherical harmonic degree 2 structure). However, the cause for and time evolution of the African and Pacific superplumes and the degree 2 mantle structure remain poorly understood with two competing proposals. First, the African and Pacific superplumes have remained largely unchanged for at least the last 300 Myr and possibly much longer. Second, the African superplume is formed sometime after the formation of Pangea (i.e., at 330 Ma) and the mantle in the African hemisphere is predominated by cold downwelling structures before and during the assembly of Pangea, while the Pacific superplume has been stable for the Pangea supercontinent cycle (i.e., globally a degree 1 structure before the Pangea formation). Here, we construct a proxy model of plate motions for the African hemisphere for the last 450 Myr since the Early Paleozoic using the paleogeographic reconstruction of continents constrained by paleomagnetic and geological observations. Coupled with assumed oceanic plate motions for the Pacific hemisphere, this proxy model for the plate motion history is used as time-dependent surface boundary condition in three-dimensional spherical models of thermochemical mantle convection to study the evolution of mantle structure, particularly the African mantle structure, since the Early Paleozoic. Our model calculations reproduce well the present-day mantle structure including the African and Pacific superplumes and generally support the second proposal with a dynamic cause for the superplume structure. Our results suggest that while the mantle in the African hemisphere before the assembly of Pangea is predominated by the cold downwelling structure resulting from plate convergence between Gondwana and Laurussia, it is unlikely that the bulk of the African superplume structure can be formed before ~230 Ma (i.e., ~100 Myr after the assembly of Pangea). Particularly, the last 120 Myr plate motion plays an important role in generating the African superplume. Our models have implications for understanding the global-scale magmatism, tectonics, mantle dynamics, and thermal evolution history for the Earth since the Early Paleozoic.

Citation: Zhang, N., S. Zhong, W. Leng, and Z.-X. Li (2010), A model for the evolution of the Earth's mantle structure since the Early Paleozoic, *J. Geophys. Res.*, *115*, B06401, doi:10.1029/2009JB006896.

1. Introduction

[2] Seismic tomography studies reveal that the present-day Earth's mantle is predominated by a largely spherical harmonic degree 2 structure that is controlled by two antipodal seismically slow velocity anomalies, one beneath Africa and the other beneath the central Pacific, separated by circum-Pacific seismically fast anomalies [*Dziewonski*, 1984; *Grand et al.*, 1997; *van der Hilst*, 1997; *Ritsema et al.*, 1999; *Masters et al.*, 2000; *Romanowicz and Gung*, 2002] (Figure 1). These two major slow velocity anomalies are sometimes referred to as the African and Pacific superplumes [e.g., *Romanowicz and Gung*, 2002]. The African and Pacific superplumes in the core-mantle boundary (CMB) regions may include significant chemical heterogeneities (i.e., chemical piles) in addition to thermal anomalies [*Su and Dziewonski*, 1997; *Masters et al.*, 2000; *Wen et al.*, 2001; *Ni et al.*, 2002, 2005; *Wang and Wen*, 2004; *He and Wen*, 2009]. The two superplumes correlate well with the geoid highs [*Hager et al.*, 1985; *Hager and Richards*, 1989], dynamic topographic highs [*Nyblade and Robinson*, 1994; *Davies and Pribac*, 1993; *Lithgow-Bertelloni and Silver*, 1998], and intraplate volcanism and hot spots in these regions [*Anderson*, 1982; *Torsvik et al.*, 2006; *Garnero et al.*, 2007].

[3] Mantle structure has broad implications for the dynamics of the mantle and lithosphere including heat transfer and long-

[1]Department of Physics, University of Colorado, Boulder, Colorado, USA.
[2]Department of Applied Geology, Curtin University of Technology, Perth, Western Australia, Australia.

0148-0227/10/2009JB006896

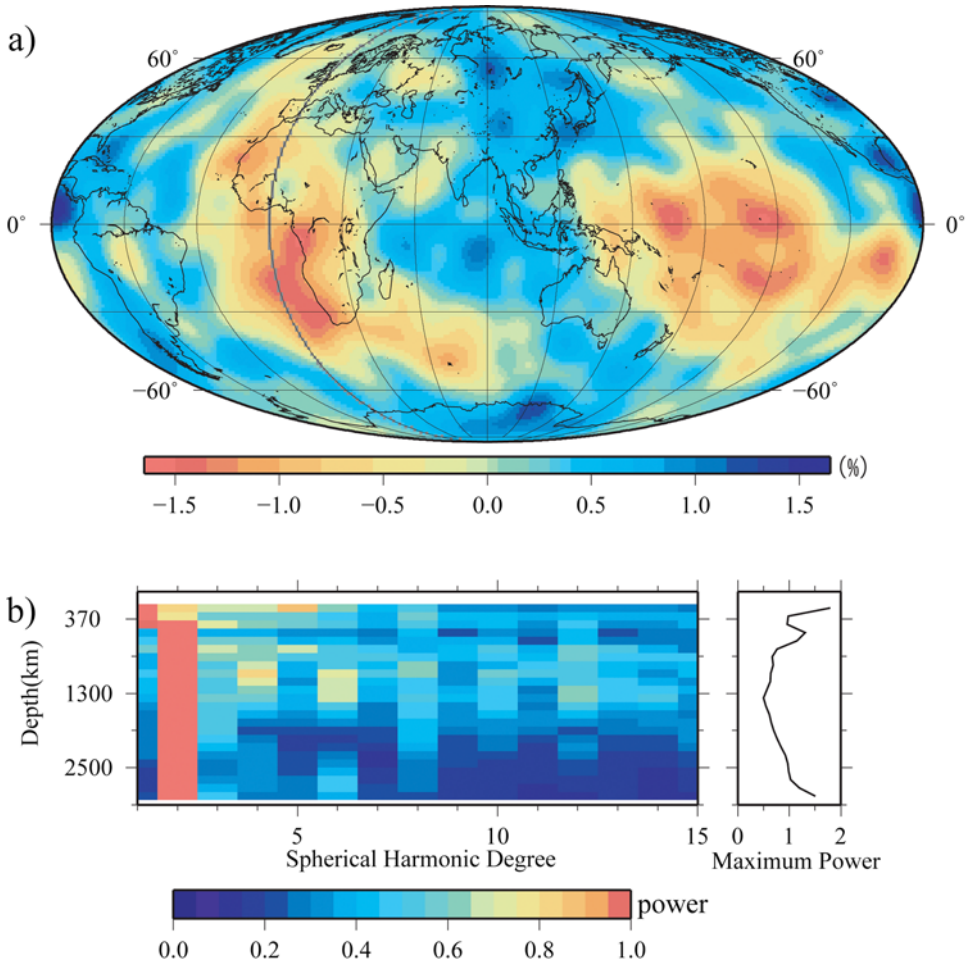

Figure 1. Shear wave velocity heterogeneity for the tomographic model S20RTS shown (a) in map view at 2750 km depth and (b) as the normalized power spectra at different depths. Figure 1b (right) shows the maximum power at different depths that is used to normalize the power.

term thermal evolution of the mantle [e.g., *Davies*, 1999; *Zhong and Gurnis*, 1994; *Grigné et al.*, 2005; *Lenardic et al.*, 2006; *Höink and Lenardic*, 2008]. Therefore, it is important to understand the cause of the degree 2 mantle structure. Surface tectonics and plate motion are thought to be closely linked to mantle structure due to mantle convection [*Hager and O'Connell*, 1981; *Anderson*, 1982; *Chase and Sprowl*, 1983]. For example, mantle convection modeling studies have demonstrated that the plate motion history for the last 120 Myr is responsible for the circum-Pacific seismically fast anomalies (i.e., subducted lithosphere) [*Ricard et al.*, 1993; *Lithgow-Bertelloni and Richards*, 1998; *Bunge et al.*, 1998] and for the two major thermochemical piles beneath Africa and the central Pacific [*McNamara and Zhong*, 2005].

[4] The present-day mantle structure cannot be fully understood without understanding its past and the dynamic evolution. Since the African superplume is located beneath supercontinent Pangea that existed between 330 and 180 Ma, it was proposed that the African superplume may have been formed during Pangea time as a result of thermal insulating effects from Pangea and that the superplume may eventually have caused the eventual breakup of Pangea [*Anderson*, 1982; *Gurnis*, 1988]. The Pacific superplume was suggested by some to have formed ~700 Myr ago during the breakup of Rodinia and has remained largely unchanged since [*Maruyama*, 1994; *Maruyama et al.*, 1997, 2007; *Condie*, 2003], mainly with evidence for the prolonged subduction zones along continental margins surrounding the paleo-Pacific [e.g., *Li and Powell*, 2001; *Scotese*, 2001]. Recognizing that most of large igneous provinces (LIPs) for the past 300 Myr erupted near the edges of the Africa and Pacific thermochemical piles, *Torsvik et al.* [2006, 2008a] suggested that the African and Pacific superplumes and the degree 2 mantle structure may have existed for the last 300 Myr. *Burke et al.* [2008] further speculated that the mantle structures may have been stable well beyond the last supercontinent cycle.

[5] Considering that supercontinent formation and breakup appear to be a cyclic process [e.g., *Nance et al.*, 1988; *Gurnis*, 1988] and that during the formation of a supercontinent, the convergence between continental blocks may lead to accumulation of subducted lithosphere beneath the supercontinent, *Zhong et al.* [2007] proposed that during and shortly after Pangea formation, the mantle in the African hemisphere is relatively cold with downwelling slabs, while the Pacific hemisphere is hot with a system of upwellings (i.e., the spherical harmonic degree 1 structure) and that such a degree 1

convective structure is the fundamental cause for Pangea formation. They suggested that the present-day degree 2 mantle structure was not formed until the African superplume was formed after Pangea formation as a result of the circum-Pangea subduction that induced upwelling return flow below Pangea, which is different from the thermal insulation mechanism by *Anderson* [1982]. *Zhong et al.* [2007] further proposed that the Earth's mantle structure may alternate between degree 1 and degree 2 planforms accompanied by supercontinent cycles. This hypothesis was motivated by the mantle convection modeling results that with relatively realistic mantle and lithospheric rheology, mantle convection is characterized by a degree 1 planform or degree 2 planform after a supercontinent is formed [*Zhong et al.*, 2007]. Recently, using models similar to those of *Phillips and Bunge* [2005, 2007], *Zhang et al.* [2009] investigated the interaction between multiple continental blocks and mantle convection of different planforms and confirmed the effect of degree 1 mantle convection on supercontinent formation.

[6] The main goals of this study are to investigate time evolution of mantle structure from pre-Pangea time to the present-day using relatively realistic paleogeographic constraints, and to test the hypothesis of alternating degree 1 and degree 2 mantle structure proposed by *Zhong et al.* [2007]. We are particularly interested in understanding how mantle structure in the African hemisphere evolves to its present-day structure. Different from *Zhong et al.* [2007], the current study includes thermochemical piles above the CMB and geologically constrained tectonic plates at the surface. Although in their two-way dynamics, intrinsic mantle convective structure has significant controls on tectonic plates [*Gurnis*, 1988; *Bercovici et al.*, 1989; *Zhong and Gurnis*, 1993; *Tackley et al.*, 1993; *Bunge et al.*, 1996; *King et al.*, 2002; *Zhong et al.*, 2007; *van Heck and Tackley*, 2008; *Foley and Becker*, 2009], inclusion of tectonic plates makes it possible to use the observations of the present-day mantle structure and of tectonic plates to constrain mantle dynamic models [e.g., *Bunge et al.*, 1998; *McNamara and Zhong*, 2005].

[7] A key component of this study is to build a proxy model for global plate motion history from the Middle Paleozoic to the present day and to use it as boundary conditions for mantle convection calculations. Although paleogeographic reconstruction of continents by *Smith et al.* [1981] was used to construct slab models for the Middle Paleozoic to study dynamic topography and global sea level variations [*Gurnis*, 1993], global plate motion models were only reconstructed back to the Late Mesozoic (119 Ma) [*Lithgow-Bertelloni and Richards*, 1998] because of the lack of adequate geological records on oceanic plates beyond that time. However, relatively consistent global paleogeographical reconstructions, based on geological and paleomagnetic information, exist for much of the Paleozoic [e.g., *Torsvik et al.*, 1996, 2008b; *Scotese*, 1997, 2001; *Reeves and de Wit*, 2000; *Li and Powell*, 2001] and can be used to constrain plate motion history since the Middle Paleozoic for the African hemisphere where all the major continental plates have been located. For oceanic plates, like those on the Pacific hemisphere, although there are geological observations suggesting for mostly divergent plate motion there since the Paleozoic [*Maruyama et al.*, 1997; *Li and Li*, 2007], there are little real constraints and we thus must rely on trying different assumptions with resulting mantle structure tested against the present-day seismic structure.

[8] This paper is organized as follows. Section two or next section describes mantle convection models with plate motion and procedures for reconstructing a proxy model for plate motion history for the last 450 Myr. Section three presents model results for mantle structure evolution under different model assumptions. Discussions and conclusions are presented in sections four and five, respectively.

2. Methods and Models

2.1. The 3-D Spherical Thermochemical Convection Models With Prescribed Plate Motion

[9] Our dynamic models of mantle convection in a three-dimensional spherical geometry assume an infinite Prandtl number and the Boussinesq approximation. Our models consider a chemical layer with different intrinsic density above the CMB, and include time-dependent plate motion as surface boundary conditions. The nondimensional governing equations for mantle convection with different compositions are [e.g., *Zhong et al.*, 2000; *McNamara and Zhong*, 2004a]:

$$\nabla \cdot \mathbf{u} = 0, \tag{1}$$

$$-\nabla P + \nabla \cdot (\eta \dot{\varepsilon}) = (\mathrm{Ra}T - \mathrm{Rb}C)\hat{e}_r, \tag{2}$$

$$\frac{\partial T}{\partial t} + (\mathbf{u} \cdot \nabla)T = \nabla^3 T + H, \tag{3}$$

$$\frac{\partial C}{\partial t} + (\mathbf{u} \cdot \nabla)C = 0, \tag{4}$$

where $\mathbf{u}$ is velocity vector, P is the dynamic pressure, η is the viscosity, $\dot{\varepsilon}$ is the strain rate tensor, T is the temperature, $\hat{e}_r$ is the unit vector in radial direction, t is the time, H is internal heat generation rate, and C is the composition that is used to define the chemical layer.

[10] Ra is the thermal Rayleigh number defined as

$$\mathrm{Ra} = \alpha \rho g \Delta T R_0^3/(\eta_r \kappa), \tag{5}$$

where α is the thermal expansivity, ρ is the density, g is the gravitational acceleration, ΔT is the temperature difference between the top and bottom boundaries, R_0 is the radius of the Earth, η_r is the reference viscosity, and κ is the thermal diffusivity. Notice that if Ra is defined by mantle thickness, d, a conversion factor, $(d/R_0)^3$, needs to be multiplied [*Zhong et al.*, 2000].

[11] Internal heat generation rate H is defined as

$$H = \frac{QR_0^2}{\rho c_p \kappa \Delta T}, \tag{6}$$

where Q is the volumetric heat production rate and c_p is the specific heat.

[12] Rb is the chemical Rayleigh number defined as

$$\mathrm{Rb} = g \Delta \rho R_0^3/(\eta_r \kappa), \tag{7}$$

where $\Delta\rho$ is the density contrast between two chemical components (e.g., chemical pile versus the mantle). A useful parameter is the buoyancy ratio, B

$$B = \mathrm{Rb}/\mathrm{Ra} = \Delta\rho/(\alpha\rho\Delta T). \quad (8)$$

The nondimensional depth- and temperature-dependent viscosity is

$$\eta(T, r) = \eta_0(r)\exp[E(0.5 - T)], \quad (9)$$

where $\eta_0(r)$ is the depth-dependent prefactor and E is the activation energy nondimensionalized by $R\Delta T$, where R is the gas constant.

[13] The nondimensional radii for the top and bottom boundaries are 1 and 0.55, respectively. Isothermal boundary conditions are applied at the surface and CMB in all calculations. For mechanic boundary conditions, the surface is prescribed with time-dependent velocity (i.e., plate motion) while the CMB is with free-slip boundary condition. The chemical layer above the CMB is assumed to be initially flat everywhere and 250 km thick [*Wang and Wen*, 2004]. Unless specified otherwise, most cases start with an 1-D initial temperature profile derived from a precalculation that uses the same parameters except that the plate motion boundary condition is replaced with free-slip boundary conditions and that a larger B for the chemical layer is used to assure that a quasi-steady state can be reached [e.g., *McNamara and Zhong*, 2005].

[14] The governing equations are solved with code CitcomS [*Zhong et al.*, 2000]) that was modified from an original Cartesian code [*Moresi and Gurnis*, 1996]. Thermochemical convection capability was incorporated into CitcomS by *McNamara and Zhong* [2004a]. The mantle is divided into 12 blocks and each block can be divided in three directions, depending on resolution [e.g., *Zhong et al.*, 2000]. For most cases, we use a grid with 12×48^3 elements, but a grid of 12×64^3 elements is also used for resolution test.

[15] Our models include five model parameters: thermal Rayleigh number Ra, depth-dependent viscosity prefactor $\eta_0(r)$, internal heat generation rate H, activation energy E, and buoyancy ratio B. Ra controls convective vigor in thermal convection with stress free boundary conditions. However, in our models with imposed plate motion, convective vigor is also dependent on the plate motion. In this study, Ra is chosen to be generally consistent with the imposed plate motion (see more in section 3.1). H is chosen to yield ~65% or 30% internal heating rate. Nondimensional activation energy E is varied from 4.61 to 9.21 to produce temperature-induced viscosity variations of 10^2 to 10^4, respectively. Although the activation energy is smaller than that from laboratory studies for olivine, it is used here for numerical stability and also to account for other weakening effects such as brittle deformation and non-Newtonian rheology. The depth-dependent viscosity prefactor $\eta_0(r)$ is specified to give rise to a viscosity jump for the lower mantle by a factor of 30 or 100 and also to possible continuous variations in viscosity with depth (i.e., pressure dependence). The last parameter, B, defines the behavior of the chemically dense layer above the CMB. The larger B is, the less entrainment mantle convection can cause to the chemical layer, and the smaller deformation or topography the chemical interface is [e.g., *Tackley*, 1998]. Details of the models will be presented in section 3.

2.2. Constructing a Proxy for Plate Motion History

[16] Our models of mantle convection include time-dependent plate motion as surface velocity boundary conditions. Here we discuss how we may construct a proxy for global plate motion history for the last 450 Myr associated with the assembly and breakup of Pangea. Based on paleomagnetic observations on the seafloor, *Gordon and Jurdy* [1986] reconstructed the global plate motion history for the Cenozoic (i.e., the last 65 Myr). *Lithgow-Bertelloni and Richards* [1998] extended the model to include the Late Mesozoic (119 Myr) using rotation poles and plate boundaries from *Engebretson et al.* [1992] and *Scotese* [1990] for the Mesozoic. Accurate reconstruction of global plate motion further back in time is not feasible due to the lack of geological records on oceanic plates, especially for the paleo-Pacific oceans or the Pacific hemisphere. However, for the African hemisphere, which has been mostly occupied by plates containing continents for the period concerned, the first order plate motion history can be constructed back to the Early Paleozoic [e.g., *Scotese*, 2001]. We adopted such reconstructions for our proxy model of plate motion history between 450 and 119 Ma. Over the same period for the Pacific hemisphere, we make assumptions for plate motion history to be discussed later. Our proxy model for the last 119 Myr uses the model of plate motion history by *Lithgow-Bertelloni and Richards* [1998].

[17] We first describe how continental plate motions are determined from Paleomap atlas of *Scotese* [2001]. A recent compilation of Phanerozoic paleogeographic reconstructions, Paleomap atlas [*Scotese*, 2001], which is broadly consistent with other recent paleographic reconstructions [*Torsvik et al.*, 1996; *Reeves and de Wit*, 2000; *Li and Powell*, 2001], has been adopted as the base maps for the 458–119 Ma interval in this study. The positions of each continental plate from one time frame to the next in the Paleomap Atlas are used to estimate the stage Euler pole and the rotation rate. We chose six time frames at 458, 390, 330, 255, 195, and 152 Ma from the Paleomap atlas to estimate the plate motion of the continental plates (Table 1). The 330 Ma frame was chosen because Gondwana and Laurussia collided at around this time to form Pangea [e.g., *Veevers*, 2004]. The plate motion between 152 and 119 Ma is determined by differencing plate positions between the 152 Ma frame in the Paleomap atlas and the 119 Ma frame from *Lithgow-Bertelloni and Richards* [1998].

[18] Identifying plate boundaries from the Paleomap atlas is important for constructing continental plate motion. We only consider major continental plates in the Paleomap atlas for our study of large-scale mantle structure. The Paleomap atlas includes four significant continental plates before Pangea formation for the time period of 458–330 Ma: Gondwana, Laurentia, Baltica, and Siberia (Figure 2a and 2b). Laurentia, Baltica, and Siberia are close to each other and they are separated from Gondwana by the Rheic Ocean. Here, we only consider two continental plates: Gondwana and proto-Laurussia which includes Laurentia, Baltica, and Siberia (Figure 2c). With this simplification, we ignore relative motions among Laurentia, Baltica, and Siberia. Here the Gondwana plate includes the Rheic Ocean and Gondwana

Table 1. Stage poles and rotational rates

Plate	Latitude	Longitude	ϖ, deg/Myr
	458–390 Ma		
Laurussia	−76	254.5	0.12
Gondwana	9	71	0.98
Paleo-Pacific1	−41.6	251.9	1.14
Paleo-Pacific2	34.7	111	1.14
Paleo-Pacific3	−31	146	1.14
Paleo-Pacific4	21.6	338.1	1.14
	390–330 Ma		
Laurussia	−85.7	259	0.19
Gondwana	12	64	1.01
Paleo-Pacific1	−46.6	256	1.14
Paleo-Pacific2	30.4	102	1.14
Paleo-Pacific3	−32	151	1.14
Paleo-Pacific4	23	332	1.14
	330–255 Ma		
Pangea	−29	65	0.14
Paleo-Pacific1	−43.4	251	1.14
Paleo-Pacific2	33	105	1.14
Paleo-Pacific3	−35.1	157	1.14
Paleo-Pacific4	23	332	1.14
	255–195 Ma		
Pangea	−18	135.6	0.4
Paleo-Pacific1	−43.4	251	1.14
Paleo-Pacific2	33	105	1.14
Paleo-Pacific3	−35.1	157	1.14
Paleo-Pacific4	23	332	1.14
Neo-Tethys	−15.8	172	0.71
	195–152 Ma		
North America	46	197	0.24
Eurasia	26	264	0.30
Gondwana	41	189	0.23
Paleo-Pacific1	−43.4	251	1.14
Paleo-Pacific2	33	105	1.14
Paleo-Pacific3	−35.1	157	1.14
Paleo-Pacific4	23	332	1.14
Neo-Tethys	−15.8	172	0.71
	152–119 Ma		
North America	57	155.4	0.59
Eurasia	31	74	0.76
South America	87.9	271	0.57
Africa and India	−14.9	135	0.51
Antarctica and Australia	−29	294	0.71
Paleo-Farallon	−43.4	251	1.14
Paleo-Pacific	33	105	1.14
Paleo-Phoenix	−35.1	157	1.14
Paleo-Izanagi	23	332	1.14

continent (Figure 2b and 2c) [*Collins*, 2003], although *Scotese* [2001] proposed a convergent plate boundary between the Rheic Ocean and Gondwana for 458 Myr ago. After Pangea formation at 330 Ma, Pangea rotates clockwise at a slow rate until its breakup ~180 Myr ago. During this period, the Paleo-Tethys Ocean is closed as south China and Indochina collide with north China, and the Neo-Tethys Ocean opens, moving Cimmeria (Turkey, Iran, and Tibet) northward [*Lawver et al.*, 2004]. In our plate motion model, we consider Pangea as a single plate from 330 to 290 Ma (Figure 2e), and introduce the Neo-Tethys plate at 290 Ma with the divergent plate boundary in the southern end of the Neo-Tethys Ocean (Figure 2f) [*Scotese*, 2001; *Lawver et al.*, 2004]. At ~195 Ma, we further divide Pangea into three plates: North America, Eurasia and Gondwana with Eurasia consisting of Baltica, Siberia, and Asian blocks (north China, south China, and Indochina) (Figure 2g). The breakup of Pangea starts as North America breaks away from Eurasia and Gondwana with the opening of the Central Atlantic Ocean (Figure 2g). Around ~152 Myr ago, Gondwana starts to break up with the openings of the South Atlantic Ocean and Indian Ocean. In our model, we replace Gondwana with three plates: South America, Africa, and Antarctica, thus ignoring the independent motions of India and Australia (Figure 2h) [*Scotese*, 2001].

[19] We considered all continental plates for the seven major time frames and obtained six sets of Euler poles and rotational rates (Table 1) and velocity vectors for all the continental plates in the African hemisphere (Figure 2). We have verified the plate motion model by comparing predicted continent positions with the Paleomap atlas [*Scotese*, 2001]. Finally, it should be pointed out that the motion of the Neo-Tethys plate is estimated from the motions of South China block and Cimmeria, relative to Gondwana [*Lawver et al.*, 2004].

[20] For oceanic plates on the paleo-Pacific hemisphere (i.e., Panthalassan) before 119 Ma, we assume that the oceanic plates have the same plate configurations and plate motion directions as those at the 119 Ma time frame in the model by *Lithgow-Bertelloni and Richards* [1998] (i.e., Izanagi, Pacific, Phoenix, and Farallon plates) (e.g., Figure 2h) with only minor adjustments to match plate boundaries (Figures 2c–2h). The average speed for these oceanic plates is assumed to be 8 cm/yr. While the circum-Pangea subduction is consistent with the Paleomap atlas [*Scotese*, 2001], this assumption implies that the Pacific hemisphere is also predominated by divergent plate motions and mantle upwellings between 458 to 119 Ma, as for the last 119 Myr. However, we also consider other plate motion scenarios for the Pacific hemisphere in later sections.

[21] For the modeling purpose, we interpolated these six time frames of plate motions before 119 Ma into a total of 23 time frames with the shortest time gap between two consecutive frames being 5 Myr. The globally averaged plate motion at different times is given in Figure 3. The average plate motion is ~6.6 cm/yr before Pangea formation at 330 Ma, but it drops to ~4.6 cm/yr at 330 Ma due to the nearly zero plate motion for Pangea at that time (Figure 2e). The increases of averaged plate motion from 330 to 240 Ma is caused by the Neo-Tethys plate motion and Pangea rotational motion (Figure 2f), while the increase at ~180 Ma reflects the breakup of Pangea. Some of the other plate motion variations in Figure 3 are caused by changes in plate geometry between different stages [*Scotese*, 2001]. The maximum plate motion of ~7.2 cm/yr occurs at ~90 Ma and the present-day averaged plate motion is ~3.9 cm/yr [*Lithgow-Bertelloni and Richards*, 1998]. Compared with the present-day plate motion of ~3.9 cm/yr, the assumed 8 cm/yr for the Pacific plates before 119 Ma leading to the globally averaged plate motion of ~6 cm/yr is reasonable, taking into the possible effects of mantle cooling on convective vigor.

[22] Finally, we emphasize that the longitudal component of plate motion for time frames before Pangea formation is not as precisely determined due to the longitudal uncertainty in paleomagnetic reconstruction of continental positions such as presented in the Paleomap atlas. However, because the convergent plate boundaries between the Pro-Laurussia and Gondwana plates are largely in the east-west direction (Figure 2c), and also because we are interested in the large-

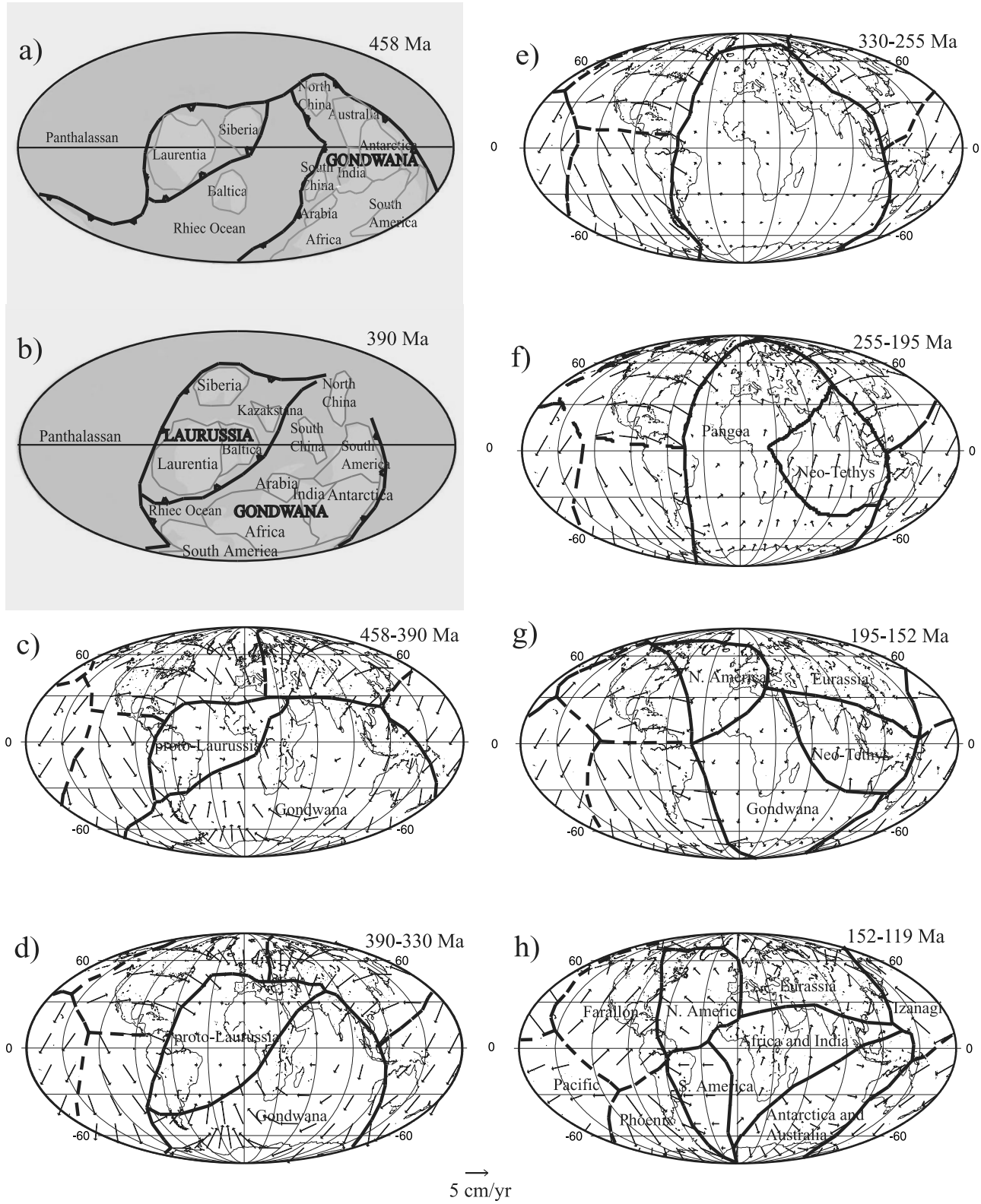

Figure 2. Reconstruction of continental plates at (a) 458 Ma and (b) 390 Ma, modified from *Scotese* [2001] and plate configuration and plate motions (arrows) during (c) 458–390 Ma, (d) 390–330 Ma, (e) 330–255 Ma, (f) 255–195 Ma, (g) 195–152 Ma, and (h) 152–119 Ma. In Figures 2a and 2b the gray lines delineate present-day continent boundaries for reference, while the light shaded regions are for the ancient continental mass. Solid and dashed lines in Figure 2c–2h represent continental and oceanic plate boundaries, respectively. The coastlines for the present day are also shown for reference.

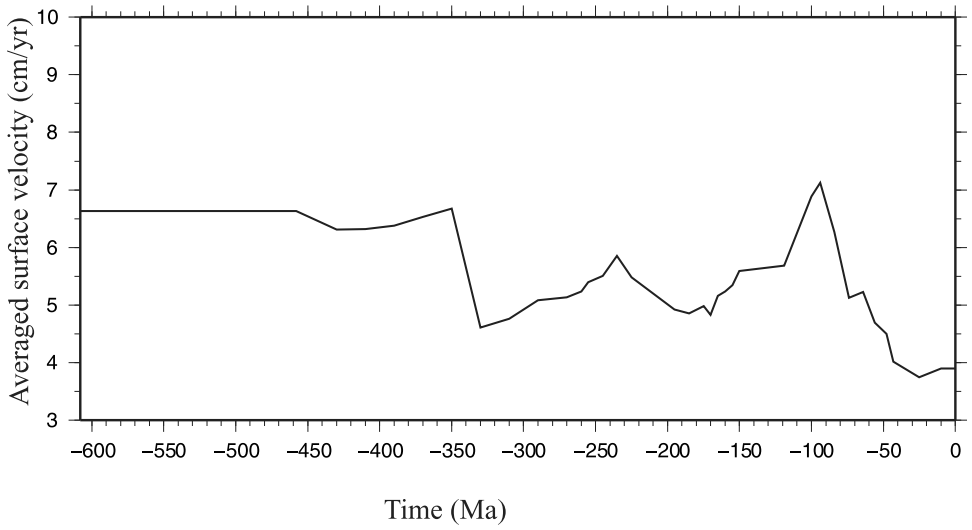

Figure 3. The globally averaged speed of surface plate motions with time.

scale mantle structure in this study, we believe that to the first order our plate motion model is sufficient.

3. Results

[23] In this section, we present model results for the time evolution of global mantle structure from Pangea time to the present-day and compare present-day mantle structure between models and seismic observations (Figure 1) [*Ritsema et al.*, 1999]. In total, 22 models are computed with different plate motion history, initial thermal structures, mantle viscosity, convective vigor and other parameters (Table 2). We focus on the evolution of the mantle in the African hemisphere in the last 450 Myr and its effects on global mantle structure.

3.1. Time Evolution of Mantle Structure for Models With Standard Plate Motions

[24] We first present 9 cases (cases FS1 to FS9 in Table 2) that include our proxy model for plate motion history from 458 Ma to the present day (Figure 2). As discussed in section 2.1, the initial thermal and chemical structures for these calculations include a 1-D temperature profile for the whole mantle and a 250 km thick chemical layer above the CMB. Model calculations for these cases start with the plate motion for the 458 Ma frame (Figure 2c), but this plate motion is maintained for 150 Myr before plate motions are updated with those for later time frames. This modeling procedure is used to take into account of the convergence between proto-Laurussia and Gondwana before 458 Ma [*Scotese*, 2001]. A similar procedure was used by *Bunge et al.* [1998] and *McNamara and Zhong* [2005] in modeling mantle structure evolution for the last 120 Myr.

[25] We start with our reference case FS1 that has Rayleigh number Ra of 2×10^8, heat generation rate H of 100, and buoyancy number B of 0.5 (Table 2). The precalculation for this case using free-slip boundary conditions yields globally averaged surface motion of 3.6 cm/yr and surface heat flux ~70 mW/m2, suggesting that the convective vigor is comparable to the Earth's mantle. A temperature- and depth-dependent viscosity is used with a nondimensional activation coefficient, $E = 9.2103$, that leads to a temperature-induced viscosity variation of 10^4. The depth-dependent viscosity includes a weak upper mantle, and a moderately strong lithosphere and lower mantle (Figure 4a), consistent with that inferred from the geoid studies [e.g., *Hager and Richards*, 1989]. The depth-dependent prefactors $\eta_0(r)$ in equation (9) for the lithosphere and the upper mantle are 1 and 1/30, respectively (Table 2). For the lower mantle, $\eta_0(r)$ increases linearly from 2.0 at the 670 km depth to 6.8 at the CMB. This leads to a mantle viscosity structure in which the lower mantle viscosity on average is ~2 orders of magnitude higher than that in the upper mantle (Figure 4a). With Ra of 2×10^8, the averaged viscosities for the upper mantle and lower mantle are $\sim 7 \times 10^{19}$ Pa s and $\sim 10^{22}$ Pa s, respectively. Case FS1 yields a globally averaged surface heat flux of ~84 mW/m^2 for the present day, comparable to the observed [e.g., *Pollack et al.*, 1993]. The internal heating rate for this case determined posterior from the surface and CMB heat flux is ~61% (Table 2), implying a significant but reasonable fraction of heating from the core [e.g., *Zhong*, 2006; *Leng and Zhong*, 2008].

[26] For case FS1, temperature fields at 2750 km depth at 458, 330, 250, 195, and 120 Ma, and for the present-day are shown in Figure 5, and 3-D mantle thermochemical structures at 330 Ma, 120 Myr ago and the present day are presented in Figure 6. Together, they show significant time dependence in mantle structures, particularly in the African hemisphere. Before Laurussia and Gondwana collides at 330 Ma to form Pangea, the convergence between these two major continental plates results in cold downwellings in the African mantle. The downwelling materials sweep the chemically dense materials to the Pacific hemisphere and below the south Gondwana to form largely a single pile above the CMB (Figures 5a, 5b, and 6a). The chemical piles accumulate below the south Gondwana because of the reduced convergence rate between Gondwana and the Pacific plates with Gondwana moving northward (e.g., Figure 2c). After the formation of Pangea, the convergence between Laurussia and Gondwana stops, and the circum-Pangea subduction causes significant reorganization of mantle structure in the African hemisphere. Particularly, subduction at the southeast side of Pangea breaks the

Table 2. Input Parameters and Outputs for Mantle Convection Models

Case	Ra	$\eta_{0\mathrm{lm}}$[a]	η (T,P)[b]	H	B	IC and BC[c]	(t_1, t_2, r)[d]	ξ[e] (%)
FS1	2×10^8	2.0	10^4(P1)	100	0.5	IC1(BC1)	(256,178,1.33)	61
FS1H	2×10^8	2.0	10^4(P1)	100	0.5	IC1(BC1)	(252,176,1.31)	60
FS2	2×10^8	3.33	10^4(P2)	100	0.5	IC1(BC1)	(271,190,1.71)	60
FS3	2×10^8	0.73	10^4(P1)	100	0.5	IC1(BC1)	(289,222,1.92)	58
FS4	2×10^8	1.33	10^4(P2)	100	0.55	IC1(BC1)	(294,235,2.07)	58
FS5	2×10^8	2.0	10^2(P1)	100	0.5	IC1(BC1)	(255,200,1.41)	63
FS6	2×10^8	2.0	10^4(P1)	100	0.6	IC1(BC1)	(263,191,1.40)	65
FS7	2×10^8	2.0	10^4(P1)	100	0.7	IC1(BC1)	(273,236,1.47)	67
FS8	2×10^8	2.0	10^4(P1)	50	0.6	IC2(BC1)	(218,123,1.11)	34
FS9	7×10^7	2.0	10^4(P1)	100	0.5	IC1(BC1)	(173,125,1.09)	66
FS10	2×10^8	2.0	10^4(P1)	100	0.5	IC1(BC2)	(243,148,1.24)	61
FS11	2×10^8	2.0	10^4(P1)	100	0.5	IC1(BC3)	(241,159,1.29)	62
FS12	2×10^8	2.0	10^4(P1)	100	0.5	IC1(BC4)	(272,184,1.76)	61
FS13	2×10^8	2.0	10^4(P1)	100	0.5	IC1(BC5)	(254,169,1.07)	59
FS14	2×10^8	1.33	10^4(P2)	100	0.55	IC1(BC5)	(275,239,1.12)	53
PS120_11	2×10^8	2.0	10^4(P1)	100	0.5	IC3(BC1)	–	62
PS220_11	2×10^8	2.0	10^4(P1)	100	0.5	IC3(BC1)	–	62
PS320_11	2×10^8	2.0	10^4(P1)	100	0.5	IC3(BC1)	–	61
PS420_11	2×10^8	2.0	10^4(P1)	100	0.5	IC3(BC1)	–	62
PS220_11V	2×10^8	0.73	10^4(P1)	100	0.5	IC3(BC1)	–	60
PS220_6	2×10^8	2.0	10^4(P1)	100	0.5	IC4(BC1)	–	61
PS320_6	2×10^8	2.0	10^4(P1)	100	0.5	IC4(BC1)	–	61
FS_L2	2×10^8	2.0	10^4(P1)	100	0.5	IC5(BC1)	(290,233,1.23)	62
PS120_L2	2×10^8	2.0	10^4(P1)	100	0.5	IC5(BC1)	–	59
PS250_L2	2×10^8	2.0	10^4(P1)	100	0.5	IC5(BC1)	–	59

[a]Value of the preexponential factor; $\eta_0(r)$, at the top of the lower mantle and the variation of $\eta_0(r)$ in the lower mantle are represented by P1 and P2, respectively. The prefactors, $\eta_0(r)$, for the lithosphere (i.e., <100 km depth) and for the upper mantle between 100 and 670 km depths are fixed at 1 and 0.0333, respectively, for all cases.

[b]The values represent the viscosity variations caused by temperature variations, while the value in parentheses represent either a factor of 3.4 linear increase in viscosity with depth across the lower mantle (P1) or no such a continuous variations with depth (P2).

[c]IB, initial conditions, and BC, boundary conditions. Five different initial conditions, IC1–IC5, and five boundary conditions, BC1–BC5, are used. BC1 stands for the standard plate motion model in Figure 2, while BC2 and BC3 are for those with 60° and 120° rotations of plates for frames before 119 Ma with respect to BC1. BC4 stands for three plates in Pacific hemisphere, while BC5 differs from BC4 in having an increased plate motion to 11 cm/yr for the Pacific hemisphere before 119 Ma. For IC1, IC2, and IC5, plate motion of 458 Ma frame is used at the beginning for 150 Myr before later frames are used. IC1 and IC2 use 1-D temperature profiles from precalculations with free-slip boundary conditions with H = 100 and 50, respectively, while IC5 uses the present-day thermal structure from the reference case FS1 as initial conditions. IC3 and IC4 are for calculations with initially downwellings in the Pacific hemisphere from 11 and 6 cm/yr plate convergence for 100 Myr, respectively. Also for IC3 and IC4, plate motion boundary condition is from FS1 but starts immediately at corresponding times.

[d]The parameters t_1 and t_2 are the times when the power of degree 2 reaches the minimum and surpasses the degree 1, respectively (see Figure 7b); r is the ratio of the power of degree 1 to degree 2 at 330 Ma.

[e]The internal heating rate.

chemical pile into two and sweeps part of the chemically dense materials toward the African hemisphere (Figures 5c and 5d). Eventually, a major hot upwelling system overriding a major chemical pile forms in the African hemisphere (Figures 5e, 5f, 6c, and 6e). The time evolution of mantle structure in the African hemisphere can also be seen from the averaged mantle temperature in the central region of the African hemisphere that increases significantly at 330 Ma and also during the last 100 Myr (Figure 7a).

[27] The mantle in the Pacific hemisphere from case FS1 is always predominated by a major upwelling system overriding a chemical pile at the CMB (Figures 5, 6b, 6d, and 6f), as a result of the assumed divergent plate motions for this hemisphere. Therefore, on a global scale, while the Pacific superplume is always present in the model, the African hemisphere is relatively cold at the time of Pangea formation and the African superplume is not formed until some time after Pangea formation. This global scale mantle structure evolution can also be seen in the power spectra of mantle temperatures at different times (Figures 7b, 8a and 8b). The mantle temperature field near the CMB is predominated by spherical harmonic degree 1 pattern during and shortly after the Pangea formation (Figure 7b), consistent with the single major upwelling system in the Pacific hemisphere during this time (Figures 5b and 6b). At 330 Ma, the degree 1 pattern dominates almost all the depths in the mantle (Figure 8a). However, the degree 1 structure starts to decrease after the Pangea formation at 330 Ma (Figure 7b). As the African upwelling system forms, the degree 2 structure starts to increase at 256 Ma and surpasses the degree 1 at 178 Ma (Figure 7b and Table 2).

[28] We now focus on present-day mantle structure from case FS1 and compare it with seismic model S20RTS [*Ritsema et al.*, 1999]. The present-day mantle structure for case FS1 compares well with the seismically observed, including the African and Pacific superplumes and the circum-Pacific subduction zones (Figure 5f and 1a). The power spectra of the temperature field for case FS1 shows that the strongest power occurs at degree 2 in the lower mantle while in the upper mantle the strongest power is at degree 3 (Figure 8b). This compares reasonably well with model S20RTS (Figure 1b). However, in model S20RTS, the degree 2 structure dominates the entire mantle except for the top 400 km where the degree 1 is more important (Figure 1b), and the degree 3 structure is not as significant as that in case FS1. This is an improvement over the models by *McNamara and Zhong*

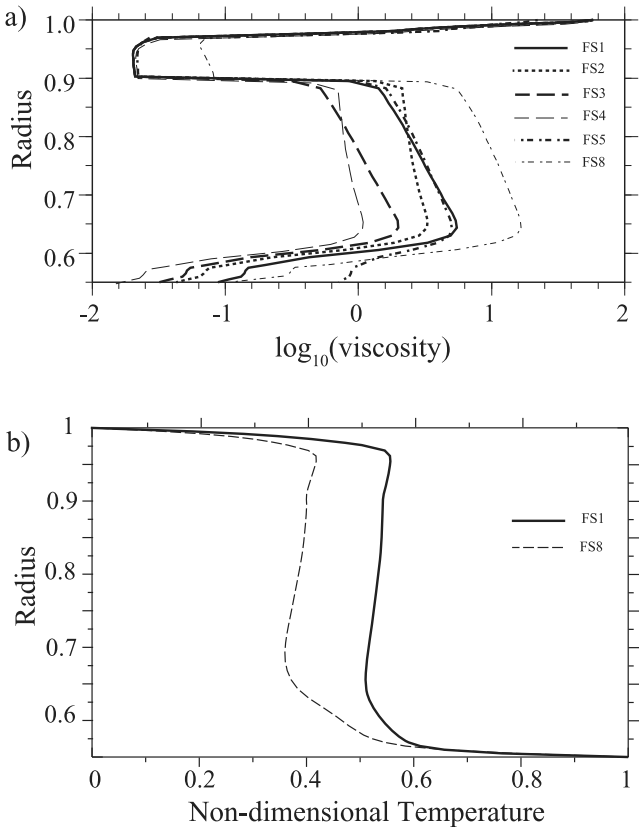

Figure 4. Depth dependences of horizontally averaged (a) mantle viscosities for cases FS1, FS2, FS3, FS4, FS5, and FS8 and (b) mantle temperatures for cases FS1 and FS8.

[2005] and *Bull et al.* [2009] that show stronger degree 3 structures than degree 2 in the lower mantle with only the last 120 Myr plate motion history. The degree correlation between model S20RTS and case FS1 shows that the best correlation occurs at the degree 1 and degree 2 in the lower mantle (Figure 8c). The upper mantle and the short wavelength structures do not correlate very well between convection and seismic models. This is also confirmed by the summed degree correlation for the first six harmonics (i.e., degrees 1 to 6) (Figure 8d). Finally, case FS1H with a higher resolution ($12x64^3$ elements) is computed and confirms the results from case FS1 (Table 2).

[29] We now present eight more cases (cases FS2–FS9 in Table 2) in which we vary the viscosity structures, buoyancy ratio B, internal heat generation H, and Rayleigh number Ra. These eight cases are used to examine the effects of the relevant model parameters on the main results from case FS1: 1) the time evolution of mantle structure, particularly mantle structure in the African hemisphere, 2) the present-day mantle structure.

[30] Cases FS2, FS3 and FS4 differ from case FS1 mainly in depth-dependent viscosity. In Case FS2, the prefactor η_r at the 670 km depth increases from 2.0 for case FS1 to 3.33 (Table 2), but case FS2 eliminates the linear increase in viscosity with depth. As a result, the averaged viscosity for the lower mantle between cases FS1 and FS2 is similar (Figure 4a). Case FS3 differs from case FS1 only in having a reduced prefactor of 0.73 at the 670 km depth while the linear increase of a factor of 3.4 across the lower mantle is kept. This leads to the lower mantle in case FS3 that is about three times weaker than that for case FS1. Case FS4 differs from case FS2 also in having 2.5 times smaller viscosity for the lower mantle, but the buoyancy number B is increased slightly to 0.55 (Table 2).

[31] Cases FS2–FS4 show similar results to case FS1 for the time evolution of mantle structure and for the present-day mantle structure (Figures 7b, 9a, and 9b for case FS3). However, while the degree 1 structures for cases FS2–FS4 start to decrease at ~330 Ma, similar to that for case FS1, the degree 2 structures for cases FS2–FS4 start to increase and surpass that at degree 1 at much earlier times than for case FS1 (Table 2). For example, the power at degree 2 surpasses that at degree 1 at 190 Ma, 222, and 235 Ma for cases FS2, FS3, and FS4, respectively, compared with 178 Ma for case FS1 (Table 2). We think that the faster development of the degree 2 structure (i.e., the African superplume structure) for cases FS2–FS4 is caused by the reduced viscosity for the bottom 1000 km of the lower mantle which makes the lower mantle flow and deform more easily. It should be pointed out that the reduced viscosity for the lower mantle enhances the entrainment for the chemically dense materials and results in reduced sizes for the present-day African and Pacific chemical piles, as evident in their thermal structures (Figure 9b for case FS3). In fact, a slightly higher buoyancy number B = 0.55 is needed in Case FS4 to prevent the chemical piles from becoming fully entrained.

[32] Case FS5 differs from case FS1 in having a reduced activation energy that gives rise to viscosity variation of 10^2 due to temperature variations, compared to 10^4 in case FS1 (Table 2 and Figure 4a). Case FS5 shows similar results for time evolution of mantle structure and the present-day structure to case FS1. However, the power at degree 2 becomes stronger than that at degree 1 at 200 Ma, earlier than that for case FS1 (Table 2). This could be due to the smaller viscosity for the bottom 1000 km of the lower mantle (Figure 4a), compared with case FS1.

[33] The buoyancy ratios B for cases FS6 and FS7 are 0.6 and 0.7, respectively, which is the only difference from case FS1 (Table 2). It is well known that a larger buoyancy ratio leads to less deformation for the chemical layer [e.g., *Davaille*, 1999; *Tackley*, 1998; *Kellogg et al.*, 1999; *McNamara and Zhong*, 2004a]. This is also observed in cases FS6 and FS7. For example, for case FS7, the CMB region affected by the downwelling slabs is much more limited (Figures 9c and 9d) than in case FS1, and the present-day structure differs significantly from the seismically observed (Figure 1). However, the power spectra for the CMB region still shows degree 1 to degree 2 structure change, although the amplitude of the power is much less than that in case FS1 (Figure 7c). A noticeable trend for cases FS1, FS6, and FS7 is that the internal heat rate increases significantly with B (Table 2), reflecting less efficient heat transfer at the CMB with increased B.

[34] Case FS8 differs from case FS1 in having a smaller internal heat generation rate (H = 50) and a larger buoyancy ratio (B = 0.6). Internal heating rate for this case is reduced to 34% compared to 61% in case FS1 (Table 2). With the reduced H, the mantle temperature for case FS8 (from the

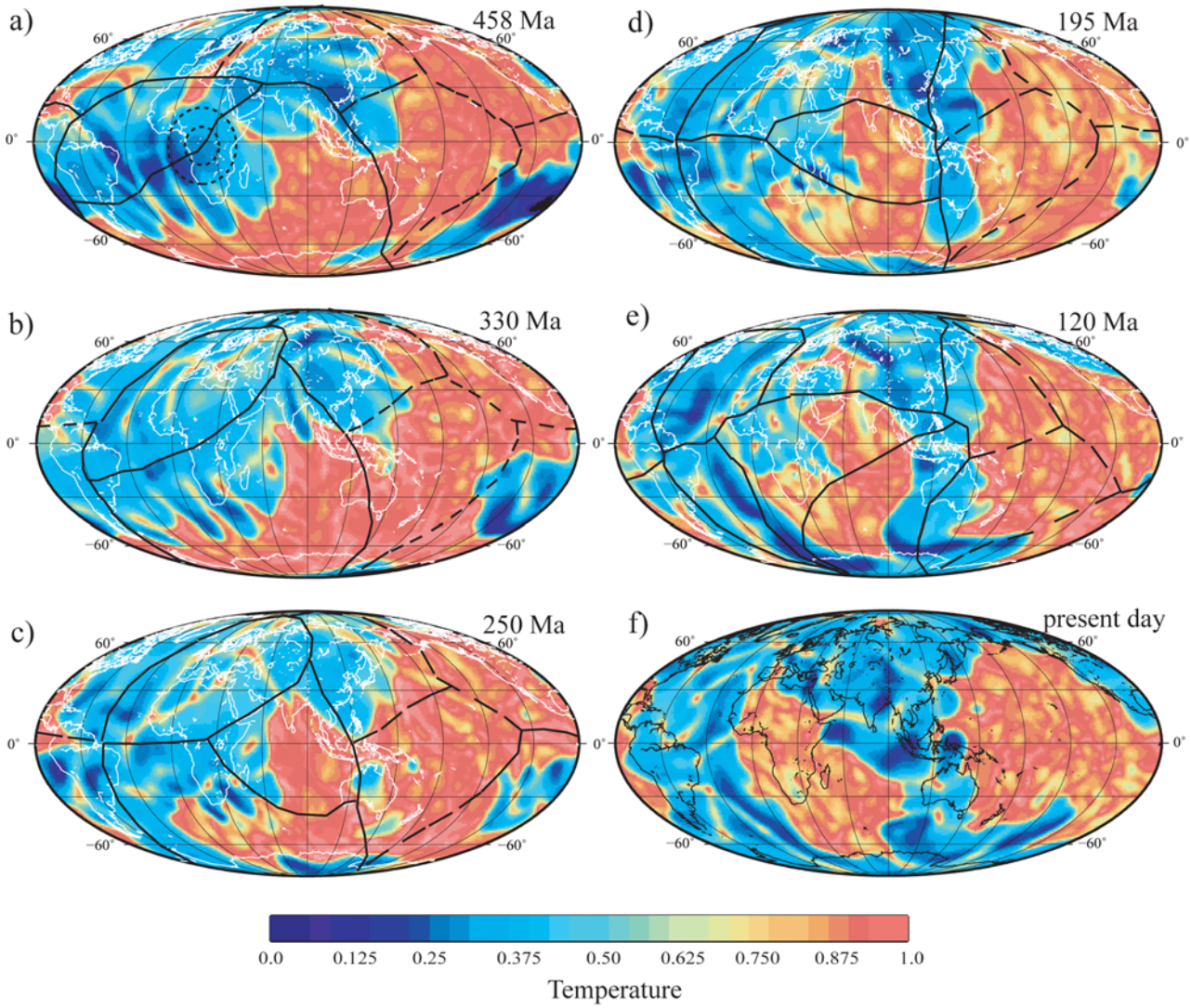

Figure 5. Snapshots of mantle thermal structures at 2750 km depth for case FS1 at (a) 458 Ma, (b) 330 Ma, (c) 250 Ma, (d) 195 Ma, (e) 120 Ma, and (f) the present day. Solid and dashed lines in Figure 5a–5e represent continental and oceanic plate boundaries, respectively. The two black dashed circles in Figure 5a mark the areas for quantifying the temperature variations in the African hemisphere shown in Figure 7a.

precalculation) is much cooler than that for case FS1 (Figure 4b), and this leads to much higher viscosity for case FS8 (Figure 4a). Case FS8 shows similar results to case FS1 for the time evolution of mantle structures and for the present-day structure (Figures 7c, 9e, and 9f). However, because of the increased mantle viscosity, the degree 2 structure forms much slower in the lower mantle for case FS8 (Figure 7c and Table 2) than for case FS1. It is also worthwhile to point out that for this case, a higher buoyancy number B is needed to reduce the entrainment of the chemical piles. This is probably because the relatively cold mantle for this case makes the chemical piles effectively more buoyant.

[35] In Case FS9, the Rayleigh number is reduced by a factor of three to Ra = 7×10^7 (Table 2), and otherwise this case is identical to case FS1. Reducing Ra is equivalent to increasing mantle viscosity uniformly. Therefore, it is not surprising to see that the formation of degree 2 structure is delayed, compared to case FS1 (Table 2). Otherwise, case FS9 shows similar results to case FS1.

3.2. Effects of Different Plate Motion and Initial Thermal Structures

[36] In cases FS1–FS9, the prescribed time-dependent surface plate motion is based on the proxy model of plate motion history for the last 458 Myr (Figure 2) that assumes four divergent plates for the Pacific hemisphere during this entire period of time. In this section, we examine the effects of this assumption on the main results, particularly the time evolution of mantle structure in the African hemisphere.

[37] We first present five cases (cases FS10–FS14 in Table 2) that differ from cases FS1–FS9 in plate configuration, Euler poles, and rotational rates for oceanic plates while the plate motions in the Pacific hemisphere are kept as divergent motions. In cases FS10 and FS11, the oceanic plate

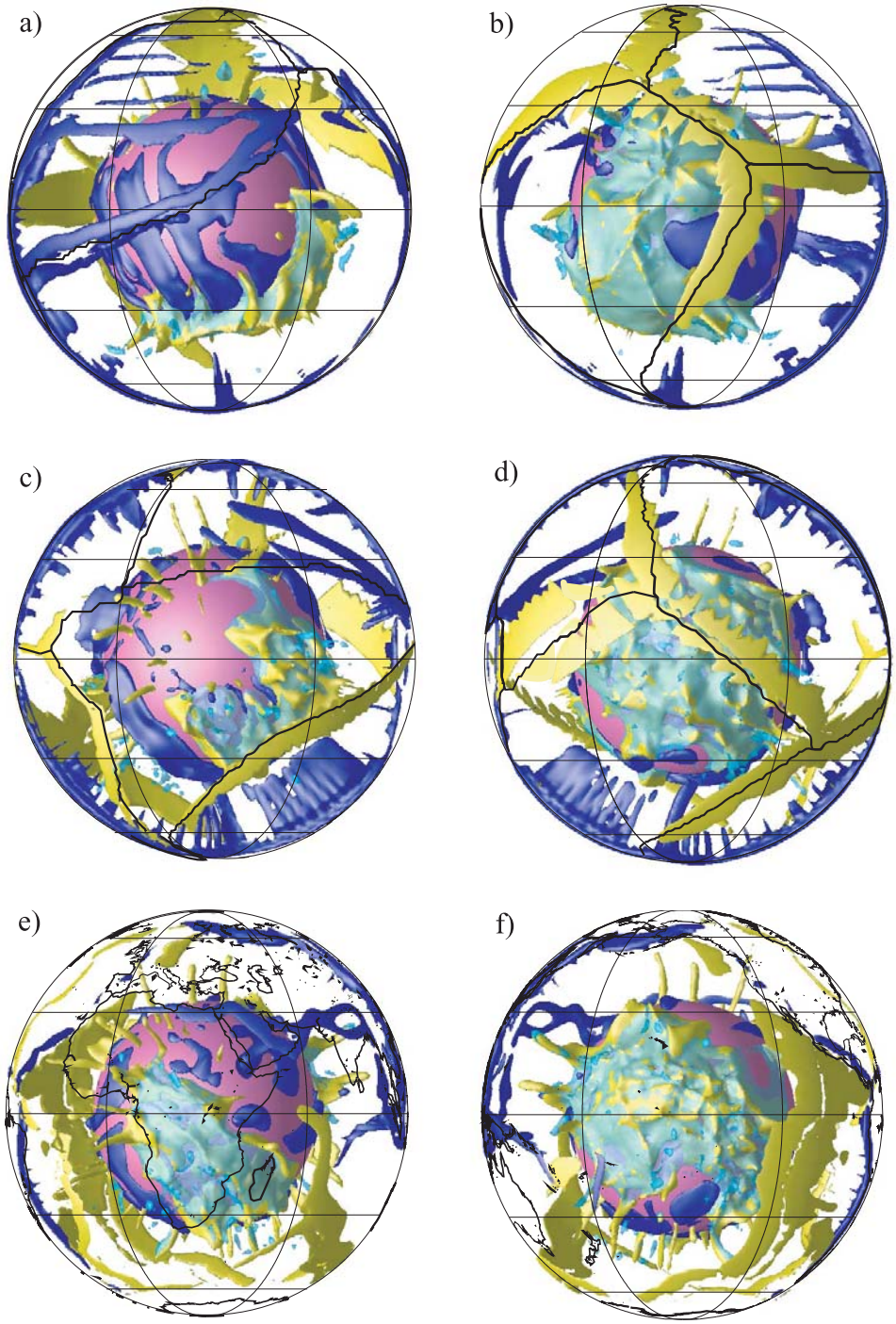

Figure 6. Three-dimensional hemispherical views of thermochemical structures for case FS1 at (a, b) 330 Ma, (c, d) 120 Ma, and (e, f) the present day. The thermal structures are plotted as isosurfaces of residual temperature with contour levels of −0.18 (blue) and 0.18 (yellow), and the chemical structures are plotted as isosurfaces of compositional field (transparent green). The core mantle boundary is plotted as a red spherical surface. Plate boundaries are plotted for the 330 and 120 Ma time frames, while for the present day the coastlines are plotted for reference. (left) Centered on longitude 30° (i.e., the African hemisphere) and (right) centered on longitude 210° (i.e., the Pacific hemisphere).

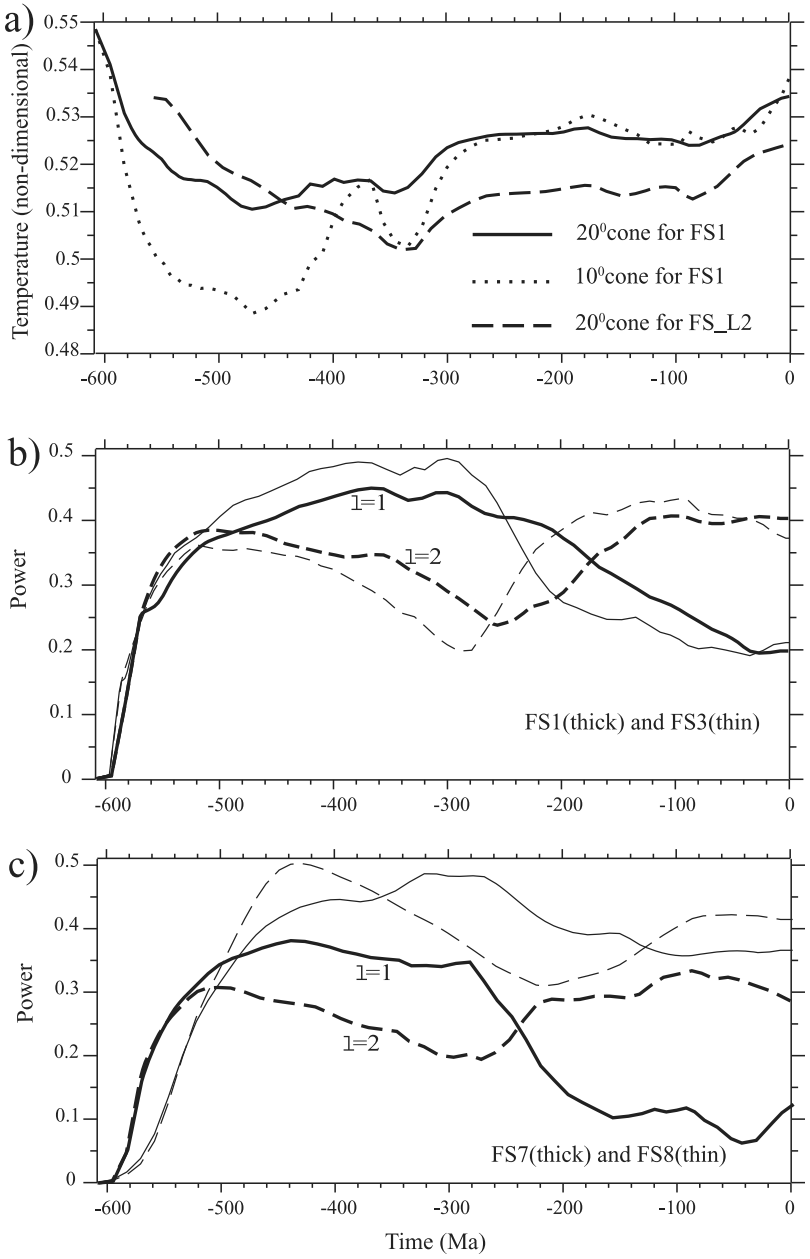

Figure 7. Time dependence of (a) averaged temperature in the African hemisphere for cases FS1 and FS_L2, (b) the powers at spherical harmonic degrees 1 and 2 for cases FS1 and FS3, and (c) FS7 and FS8. In Figure 7a, the temperatures are averaged for the mantle over the areas shown in Figure 5a.

configurations and plate motions in the Pacific hemisphere before 119 Ma are rotated by 60° and 120°, respectively, compared with that used in case FS1. For cases FS10 and FS11, the oceanic plates are assigned with new Euler poles but keep the same rotational rates as those in case FS1. Cases FS10 and FS11 are otherwise identical to case FS1. The general results from cases FS10 and FS11 (Figures 9g and 9h for case FS11) are similar to those for case FS1, although the African superplume and degree 2 structure appear to form later than those in case FS1 (Table 2). We did not compute other cases with further rotations for the oceanic plates, because with the plate configurations used here, further rotation would give rise to plate motions similar to that in either case FS1, FS10 or FS11.

[38] Case FS12 differs from case FS1 in that the Pacific hemisphere before 119 Ma is divided into three plates with a triple junction at the center of the Pacific hemisphere, while case FS1 includes four plates in the Pacific hemisphere (Figures 2c–2h). One spreading center that forms the triple junction goes through the South Pole, while the other two spreading centers are at 120° and 240° angles from the first one. Case FS12 also shows similar time evolution of mantle structures to that for case FS1 while the formation of degree 2 structure (i.e., the African superplume) is earlier by ~6 Myr than that in case FS1 (Table 2).

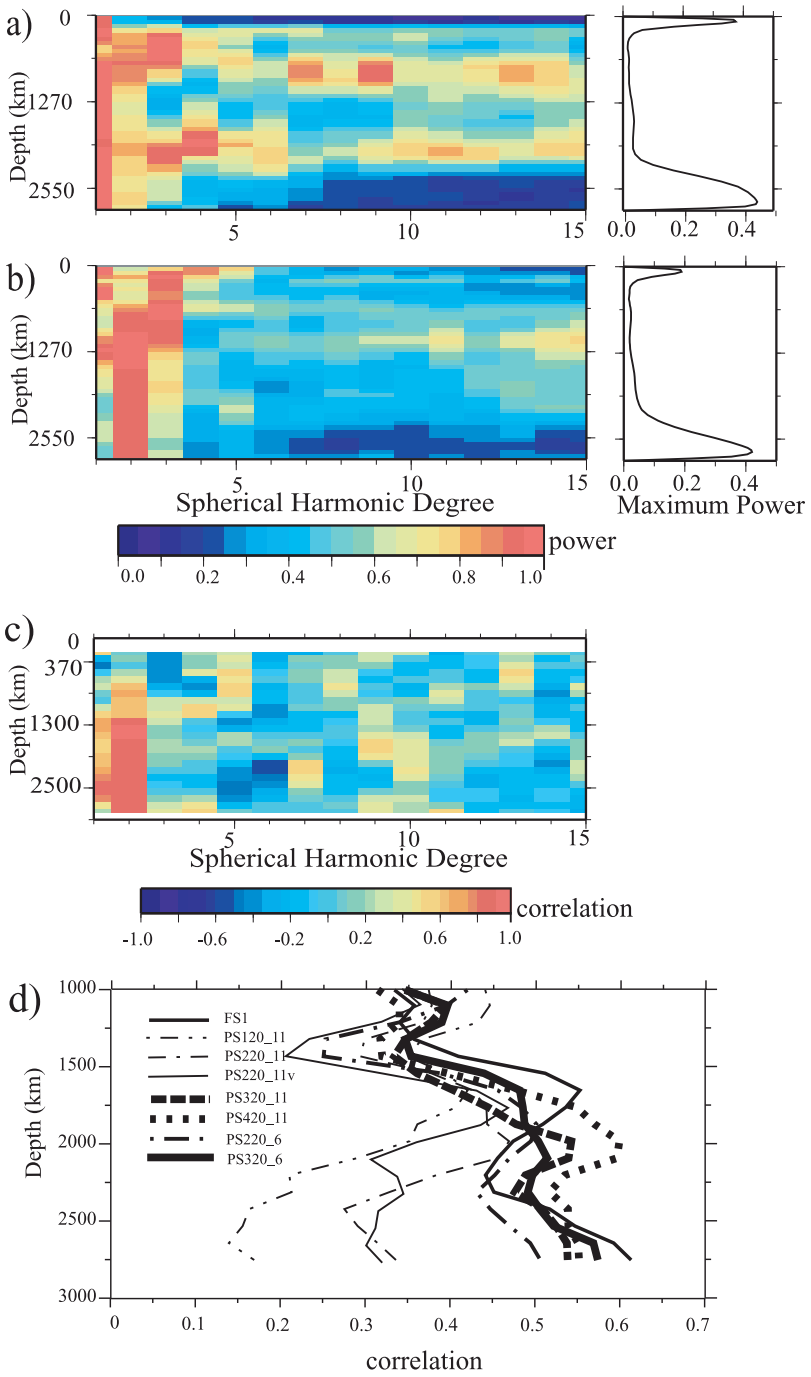

Figure 8. Normalized power spectra at different depths for the temperature fields from case FS1 at (a) 330 Ma and (b) the present day, (c) degree correlations between model S20RTS and the present-day temperature field of case FS1 at different depths, and (d) the sum of degree correlations for degrees 1 to 6 at different depths for different cases. Figure 8a (right) and 8b show the maximum power at different depths.

[39] Case FS13 differs from case FS12 only in having an increased average plate motion of 11 cm/yr for oceanic plates in the Pacific hemisphere before 119 Ma, compared to 8 cm/yr in case FS12 and other previous cases. Compared with cases FS12 and FS1, case FS13 shows a weaker degree 1 structure at 330 Ma, relative to the degree 2 (Table 2). However, the formation of the degree 2 structure and African superplume is still delayed compared with cases FS12 and FS1 (Table 2).

[40] Notice that case FS4 with a reduced viscosity in the lower mantle (Figure 4a) produces the degree 2 structure and African superplume the earliest at 235 Ma (Table 2), we computed Case FS14 that differs from case FS4 only in plate motions and plate configurations that are the same as those

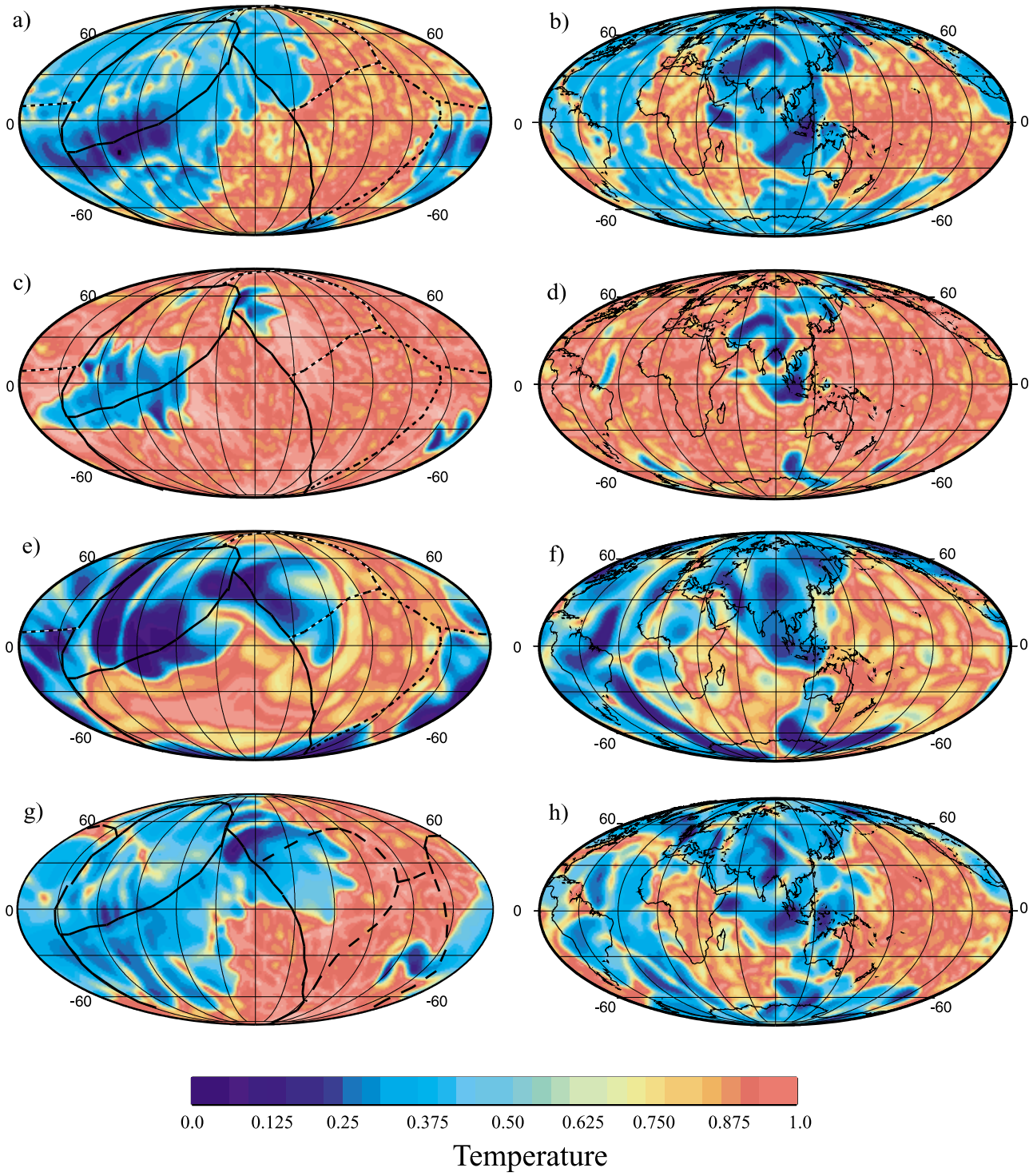

Figure 9. Temperatures at 2750 km depth at 330 Ma (left column) and the present day (right column) for cases (a, b) FS3, (c, d) FS7, (e, f) FS8, and (g, h) FS11.

in case FS13 (i.e., three plates in the Pacific hemisphere with 11 cm/yr average plate speed before 119 Ma) (Table 2). Case FS14 produces the degree 2 structure and African superplume at 239 Ma, only 4 Myr earlier than in case FS4 but ~70 Myr earlier than in case FS13 (Table 2), suggesting an important role of the lower mantle viscosity in forming the African superplume structure.

[41] Our calculations so far assume divergent plate motions in the Pacific hemisphere. Although this assumption does not significantly affect our results on time evolution of mantle structure in the African hemisphere, it is responsible for producing the upwelling system in the Pacific hemisphere and hence the degree 1 structure in our models. Although such an assumption is consistent with geological evidence for

the prolonged subduction zones along continental margins surrounding the paleo-Pacific [e.g., *Li and Powell*, 2001; *Scotese*, 2001], we will further examine the effects of the assumption on our models. To address this issue, we pose the following question: supposing that plate convergence had occurred over some period of time in the past in the Pacific hemisphere, how would the subsequent divergent plate motion in the Pacific hemisphere erase the influence of the plate convergence and produce the present-day mantle structure with the Pacific superplume?

[42] We first compute a case with the plate convergence of 100 km thick plates at a convergence rate of 11 cm/yr for 100 Myr in the Pacific hemisphere to produce an initial downwelling there (Figure 10a). We then calculate four cases that use this Pacific downwelling structure as initial thermal condition but with our proxy model for plate motion history starting from 120, 220, 320, or 420 Ma, respectively (cases PS120_11, PS220_11, PS320_11, and PS420_11 in Table 2). Other than the initial thermal structure and different plate motion history, these four cases use the same model parameters as case FS1. Calculations from these four cases show that with the initial Pacific downwelling structure (Figure 10a), plate motions for the last 320 Myr with divergent plate motions in the Pacific hemisphere may still not erase the cold structure in the Pacific to reproduce the seismic structure (Figures 10b, 10c, and 10d). In case PS320_11, while the overall structure at the CMB is similar to the present-day mantle structure, a 30° wide cold anomaly remains in the central Pacific (Figure 10d) that differs significantly from the seismic structure. However, case PS420_11 with the last 420 Myr plate motion history reproduces the present-day CMB structure well (Figure 10e). The degree correlation between the modeled present-day structures and the S20RTS model shows that for the bottom 1000 km of the mantle, the correlation is generally better than 0.5 for cases PS320_11 and PS420_11, while the correlation is significantly degraded for other two cases with shorter times of plate motion (Figure 8d).

[43] We computed three additional cases to examine the effects of an initially weaker Pacific downwelling and a lower mantle with reduced viscosity. Cases PS220_6 and PS320_6 (Table 2) use an initial Pacific downwelling that is created with 6 cm/yr plate convergence for 100 Myr in the Pacific hemisphere (Figure 10f). In cases PS220_6 and PS320_6, plate motion history for the last 220 and 320 Myr are used, respectively. With reduced initial Pacific cold anomalies, it appears that more than 220 Myr plate motion history is needed to reproduce the present-day mantle structure (Figures 10g and 8d), given that the degree correlation for case PS220_6 is generally less than 0.5 in the lower mantle. However, case PS320_6 reproduces the present-day structure well (Figures 10h and 8d). Considering the result from cases FS1–FS9 that the formation of the present-day African structure is more rapid for the lower mantle with a smaller viscosity, we computed case PS220_11V that is the same as PS220_11 except that the lower mantle viscosity is reduced by a factor 2 (i.e., the viscosity for case FS3). However, we found that the reduced viscosity for the lower mantle remains unable to reproduce the present-day mantle structure (Figure 8d).

[44] In short, this series of calculations with initial cold downwellings in the Pacific hemisphere suggest that if plate convergence had occurred in the central Pacific region, it may not have occurred in the last 220 Myr, most likely not in the last 300 Myr, for geologically reasonable convergence rates for oceanic plates (i.e., >8 cm/yr convergence rate for over 100 Myr).

[45] We now present three calculations (cases FS_L2, PS250_L2, and PS120_L2 in Table 2) to examine how the African superplume structure, if it exists in the geological history (e.g., before the Pangea), responds to the plate motion history in our proxy model. These calculations have implications for the hypotheses of long-term stability for the African and Pacific superplume structure [*Burke et al.*, 2008; *Torsvik et al.*, 2008a]. Case FS_L2 differs from case FS1 only in the initial thermochemical structure which is taken from the present-day thermochemical structure of case FS1 with the well developed African and Pacific superplumes (Figure 5f, 6e, 6f, and 11a). The purpose is to examine how the imposed plate convergence between Laurussia and Gondwana and the resulting cold downwelling slabs before Pangea formation would affect the initially prescribed African superplume structure. We found that the initially prescribed African superplume structure is greatly displaced southwards by the downwelling slabs and is largely erased by the time of Pangea formation (Figure 11b and 11d). In fact, at the time of Pangea formation and for the present day, the mantle structures from case FS_L2 are very similar to those from case FS1 at the corresponding times (Figures 11b and 11c). The smaller size for the African structure at the present day for case FS_L2 (Figure 11c), compared to its initial structure (Figure 11a), is caused by the entrainment.

[46] Cases PS250_L2 and PS120_L2 use the same initial condition (i.e., two superplumes) as in case FS_L2, but are computed with plate motion history for the last 250 and 120 Myr (i.e., after the Pangea formation), respectively. We found that for these two cases, the plate motion history for the last 120 and 250 Myr does not significantly modify the overall structures of the African and Pacific superplumes (Figures 11e and 11f), compared to their initial structures (Figure 11a). However, the positions and boundaries of the superplumes are not stationary. For example, in case PS120_L2, the west boundary of the African superplume or chemical pile migrates westward by ~20° for the last 120 Myr (Figure 11f). In case PS250_L2, the west boundary of the African pile first migrates eastward for ~15° between 250 and 170 Ma and then reverses the direction to migrate back to nearly its initial positions at the present day (Figure 11e). Therefore, cases FS_L2, PS120_L2 and PS250_L2 with initially two superplumes and chemical piles further demonstrate that the chemical piles dynamically interact with mantle flows.

4. Discussion

[47] In this study, we constructed a proxy model of global plate motion for the last 450 Myr in which the continental plates for the African hemisphere are constrained by published paleogeography of continents, while the oceanic plates for the Pacific hemisphere are assumed to be predominated by divergent plate motions. Using the plate motion model as time-dependent velocity boundary conditions in 3-D global mantle convection models, we examined the time evolution

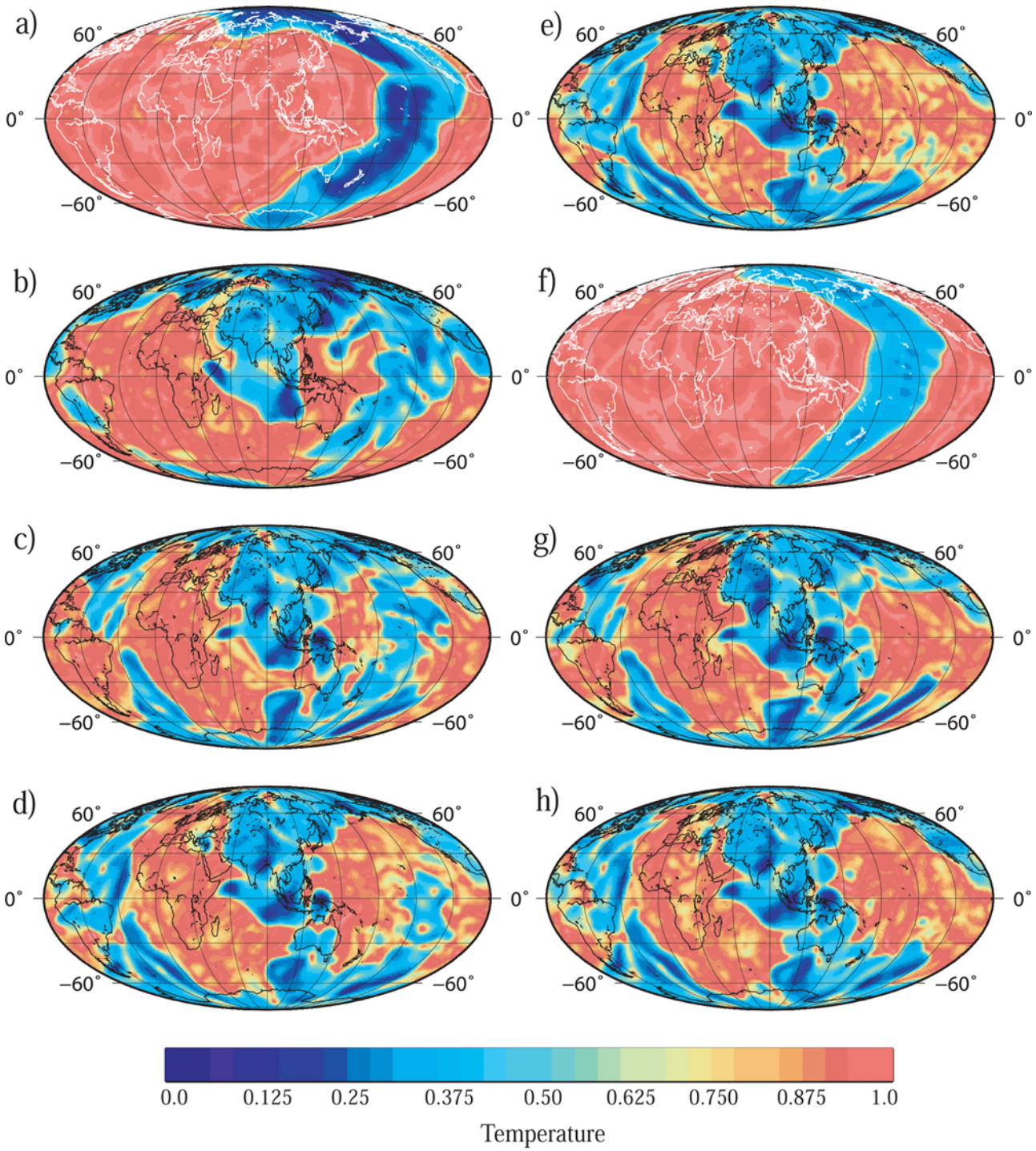

Figure 10. Temperatures at 2750 km depth (a) as initial temperature fields for cases PS120_11, PS220_11, PS320_11, and PS420_11, and the present-day thermal structures for (b) case PS120_11, (c) PS220_11, (d) PS320_11, and (e) PS420_11. (f) The initial temperature field for cases PS220_6 and PS320_6 and (g) and (h) the present-day thermal structures for cases PS220_6 and PS_320, respectively.

of the mantle structure, particularly for the African hemisphere, for the last 450 Myr and tested the hypothesis by *Zhong et al.* [2007] that cold downwelling flows having predominated the African hemisphere during Pangea formation have been replaced with hot upwellings after Pangea formation and that the global mantle structure has changed from largely degree 1 to degree 2 planforms accordingly. Here we discuss the implications of our main results for mantle dynamics in the African hemisphere and on the global scale.

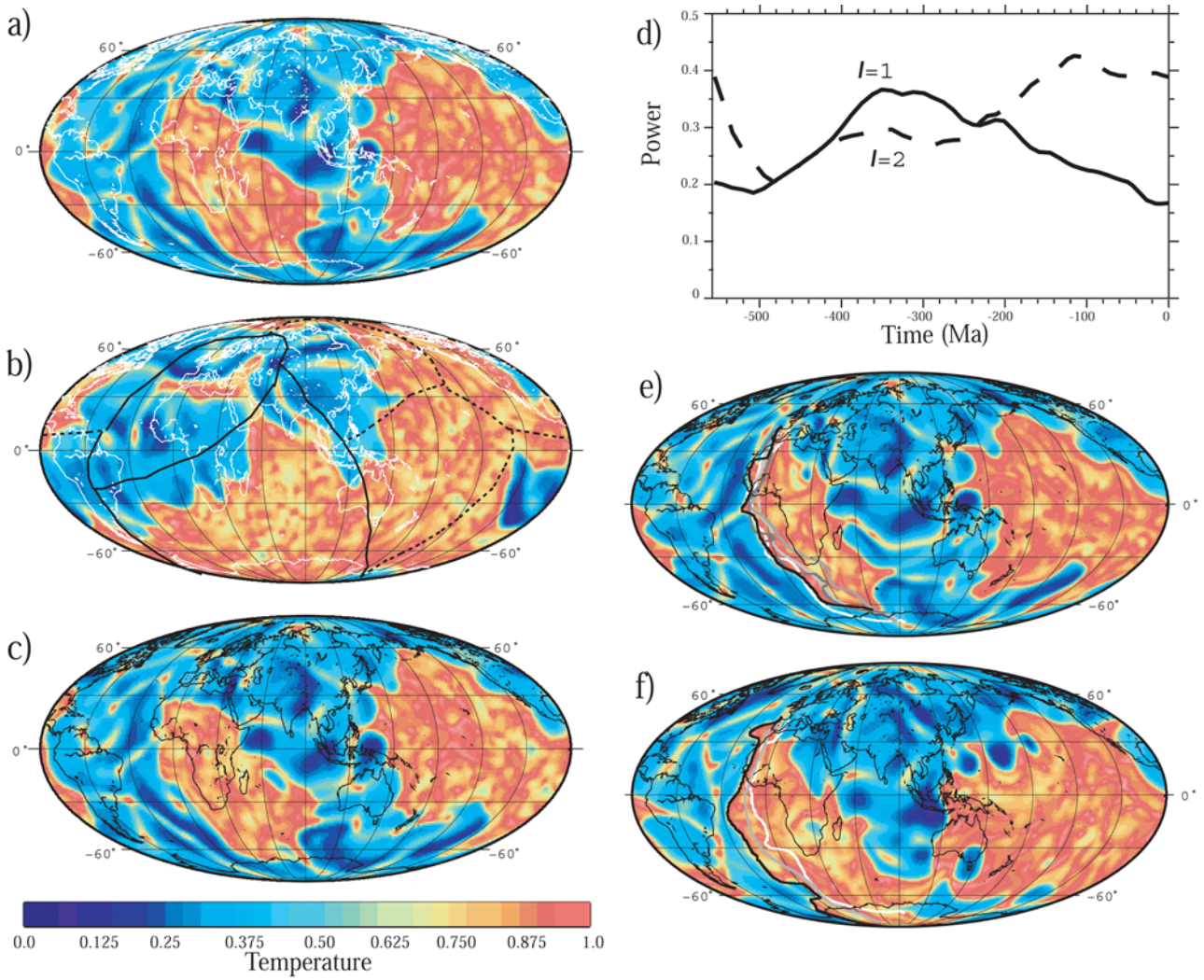

Figure 11. Temperatures at 2750 km depth for case FS_L2 (a) as initial temperatures, at (b) 330 Ma and (c) the present day, and (d) its time-dependent power spectra, and for the present-day structure for cases (e) PS250_L2 and (f) PS120_L2. In Figure 11e, the west boundary of the African superplume is shown at 250 Ma (white), 220 Ma, 170 Ma (the easternmost line), 120 Ma, and the present day (black). In Figure 11f, the west boundary of the African superplume is shown at 120 Ma and the present-day (black).

4.1. Time Evolution of the African Mantle Structure Since the Time of Pangea

[48] Our 3-D mantle convection models with the plate motion history for the last 450 Myr demonstrate that during and sometime after the Pangea formation, the mantle including the CMB regions in the African hemisphere is predominated by the cold slabs accumulated over 200 Myr of plate convergence between Gondwana and proto-Laurussia that eventually leads to the formation of Pangea. The bulk of the African superplume including its underlying chemical pile is formed after the Pangea formation over some period of time that depends on model parameters, particularly the lower mantle viscosity. We believe that our modeled mantle structural evolution for the African hemisphere is robust because the plate motion history for the African hemisphere used in our models that plays a dominant role in shaping the mantle structure in the African hemisphere is geologically and paleomagnetically constrained [e.g., *Scotese*, 2001].

[49] Our model results are consistent with the widely accepted notions that subduction over long geological times cools the mantle below, as evident in the seismic structure for the circum-Pacific mantle [e.g., *Hager et al.*, 1985; *Ricard et al.*, 1993; *Lithgow-Bertelloni and Richards*, 1998; *Bunge et al.*, 1998], and that the cold downwellings upon reaching the CMB sweep aside chemical piles [e.g., *Tackley*, 1998; *Kellogg et al.*, 1999; *Jellinek and Manga*, 2002], as evident in the African and Pacific chemical piles [*McNamara and Zhong*, 2005]. The latter arises because with the liquid outer core, the CMB is a mechanically free-slip boundary over which chemically dense piles migrate readily in response to mantle downwelling flows, even for chemical piles with high viscosity [*McNamara and Zhong*, 2004a, 2004b]. That

plume sources migrate above the CMB in response to mantle flows is also consistent with studies on the relationships between hot spot tracks, mantle flow, and seismic tomography models [*Boschi et al.*, 2007; *Steinberger and Antretter*, 2006; *Steinberger and O'Connell*, 1998] and plume dynamics [e.g., *Lenardic and Kaula*, 1994].

[50] Our result that the African mantle is predominated by cold downwellings during the Pangea formation but subsequently becomes hot after the Pangea formation is generally consistent with that proposed by *Zhong et al.* [2007] but does not support the suggestion by *Burke et al.* [2008] that the African superplume structure may have remained unchanged during the last supercontinent cycle and beyond. Here, case FS_L2 is particularly relevant and revealing, as this case demonstrates that an African superplume structure, even if existing before Pangea formation, could not have survived the cold downwelling flows from convergent plate motions between Laurussia and Gondwana (Figures 11a–11d).

[51] How and when the African superplume structure is formed in relation to the Pangea supercontinent cycle is an important question with implications for continental magmatism and tectonism for the last 300 Myr. Our models show that the formation of the African superplume depends on the lower mantle viscosity and also modestly on oceanic plate motions (Figure 7 and Table 2). However, based on the models that we have calculated so far for this study, it is unlikely that the bulk of the African superplume could have been formed earlier than 240 Ma, although individual mantle plumes could occur earlier (Figures 5 and 7 and Table 2). Furthermore, the plate motion history for the last 120 Myr plays an important role in placing the African superplume structure at its present-day location (Figures 5e and 5f). This is consistent with *McNamara and Zhong* [2005], who demonstrated that the main features of the African superplume could be reproduced from the last 120 Myr plate motion alone.

[52] The relatively young age for the African superplume structure and its dynamic nature from our models (e.g., cases FS1, PS120_L2 and PS250_L2, Figures 5, 11e, and 11f) may also pose challenges to the proposal that the African superplume and its underlying chemical pile may have remained unchanged for the last 300 Myr on the basis of studies of a large igneous province of that age [*Torsvik et al.*, 2006, 2008a, 2008c]. *Torsvik et al.* [2006] showed that most of LIPs for the last 252 Myr at their eruption times are located above the edges of the Pacific and African superplume structures [also see *Thorne et al.*, 2004] or, more specifically, near the 1% contour lines of seismic velocity anomalies above the CMB in the mean model by *Becker and Boschi* [2002] (i.e., the large low shear wave velocity provinces or LLSVPs, as *Garnero et al.* [2007] referred). They suggested that LIPs are derived from the edges of LLSVPs that are stable for at least the last 252 Myr. Recently, *Torsvik et al.* [2008c] suggested that the 298 Ma old Skagerrak-centered LIP may also be related to LLSVPs, and further proposed that LLSVPs are stable for the last 300 Myr.

[53] While more studies from both observational and physical mechanism aspects are needed to further test Torsvik *et al.*'s model, we also believe that their model warrants further deliberations. First, it is unclear how the model that LLSVPs are stable for the last 300 Myr explains the uneven temporal distribution of LIPs events during the Pangea supercontinent cycle [e.g., *Prokoph et al.*, 2004; *Li and Zhong*, 2009]. LIP events only became frequent at ~200 Myr ago (i.e., shortly before the Pangea breakup), and most of them occurred between 150 and 50 Ma [e.g., *Larson*, 1991; *Torsvik et al.*, 2008a]. Between 330 and 200 Ma, there were only three well-documented LIPs globally: Skagerrak, Emeishan, and Siberia Traps. Second, some significant LIPs including Columbia River, Greenland-Iceland, Emeishan, and Siberia Traps, are not obviously related to LLSVPs. Particularly relevant to the issue of long-term stability for LLSVPs are the Emeishan LIP and the Siberia Traps because of their > 250 Ma ages. *Torsvik et al.* [2006, 2008a] attributed the Emeishan LIP to the Pacific LLSVP, and the Siberia Traps to a small patch of moderate low-speed anomalies that is >40° away from the African LLSVP. However, recent work in south China demonstrates that the paleo-Pacific plate may have started to subduct westward under south China since at least circa 270 Ma [*Li et al.*, 2006; *Li and Li*, 2007], thus putting south China outside the Pacific hemisphere. The occurrence of LIPs away from the present-day LLSVPs may reflect the dynamic nature of LLSVPs as our modeling would imply.

[54] It should be pointed out that understanding the temporal and spatial distribution of magmatism during the Pangea supercontinent cycle has been a subject of study in geodynamics for many years. *Anderson* [1982] suggested that thermal insulating effects from Pangea could lead to increase in mantle temperature below Pangea, thus explaining the post-Pangea magmatism. Following Anderson's idea and based on 3-D convection models with purely internal heating, *Coltice et al.* [2007] recently proposed that the increased temperature below a supercontinent could reach to 100 K over a large area and lead to widely distributed volcanisms without mantle plumes. However, our study (Figure 7a) and also *Zhong et al.* [2007] show that mantle temperature below Pangea is mostly controlled by convective heat transfer that is related to plate motions with Pangea's insulating effects as secondary, also consistent with *O'Neill et al.* [2009]. The mantle below Pangea is relatively cold when Pangea was first formed due to the cold downwellings from the plate convergence between Laurussia and Gondwana, and it warms up later mostly due to the upwelling return flow in response to circum-Pangea subduction (Figure 7a). That the mantle below Pangea is cold at Pangea formation from our models suggests that additional heating may be needed for *Coltice et al.*'s [2007] model to generate widespread melting below Pangea. How our dynamic models address the issue of the temporal and spatial distribution of magmatism during the Pangea supercontinent cycle needs to be further examined.

4.2. Time Evolution of the Global Mantle Structure

[55] Our models show that the mantle in the Pacific hemisphere is predominated by a hot upwelling system from Pangea time to the present day. However, mantle structural evolution for the Pacific hemisphere is dictated by the assumed divergent plate motion for the last 450 Myr there. Although this assumption is supported, to some extent, by reconstruction of the plate motion and plate age for the Pacific seafloor for the last 140 Myr [e.g., *Muller et al.*, 2008; *Lithgow-Bertelloni and Richards*, 1998] and by the existence of subduction systems along paleo-Pacific margins for much of the Paleozoic [e.g., *Li and Powell*, 2001; *Scotese*,

2001], we consider our results for the Pacific hemisphere for the early times are not as well constrained as that for the African hemisphere where the plate motions are better known. If our result for the hot, upwelling system for the Pacific hemisphere is correct, then in conjunction with the time evolution of mantle structure in the African hemisphere, our models suggest that the global mantle structure is largely degree 1 during Pangea formation and later turns into degree 2 when the African superplume structure is formed (Figure 7b). This is consistent with the hypothesis of degree 1 to degree 2 mantle structure transition associated with supercontinent cycles proposed by *Zhong et al.* [2007].

[56] We attempted to put a constraint on the timing of when the Pacific hemisphere must have become a major upwelling system like the present day, by correlating the present-day seismic structure with the modeled in cases that employ an initially cold downwelling structure in the Pacific hemisphere and our proxy plate motion model. We found, not surprisingly, that the answer depends on the strength of the initial cold downwelling structure employed in the model (Figure 10). However, it appears that the present-day Pacific mantle structure would be inconsistent with existence of a significant plate convergence (e.g., ~10 cm/yr convergence rate for 100 Myr) in the Pacific hemisphere for the last 300 Myr. Here, it is interesting to point out that our results of possibly ~300 Myr long memory time for mantle convection with a given plate motion history are quite different from that of *Bunge et al.* [1998], who suggested that the present-day mantle structure may not depend on mantle structure from ~150 Ma.

4.3. Comparison With the Present-Day Mantle Structure

[57] Our reference model (case FS1) and other models with similar buoyancy numbers (e.g., cases FS2 and FS3) reproduce the present-day seismic structure including the degree 2 structure, the African and Pacific superplumes, and circum-Pacific cold anomalies in the lower mantle (Figures 5f, 1b, 8b, 8c, 8d, and 9b). Earlier models using similar modeling methods but a shorter plate motion history (i.e., 120 Ma) also reproduced the main features of the African and Pacific superplumes [*McNamara and Zhong*, 2005; *Bull et al.*, 2009], but these models also produced slightly stronger degree 3 structure than degree 2 near the CMB and cold downwelling structure below Africa, inconsistent with the seismic models. Our models overcome these two difficulties, suggesting that our proxy plate motion model with a longer history (~450 Ma) helps explain the present-day mantle structure. Is the entire 450 Myr plate motion history needed to reproduce the present-day mantle structure? It appears that even with some preexisting structure such as downwellings in the Pacific mantle that differs significantly from the present day, ~300 Myr history of plate motion is sufficient to reproduce the present-day mantle structure (Figure 8d). However, models with larger buoyancy numbers (e.g., case FS7) may not work as well, because they lead to too small downwelling regions at the CMB (Figure 9d), compared with seismic tomography models (Figure 1a) [*Ritsema et al.*, 1999] and seismic observations of postperovskite regions at the CMB [*Lay and Garnero*, 2007; *van der Hilst et al.*, 2007].

[58] Comparing the present-day mantle structures between the dynamic and seismic models, we found that the correlations for depths shallower than 1500 km and also near 2300 km depth are not as good as those at other depths (Figure 8d). Especially, convection models show strong degree 3 structure above 1200 km depth (Figure 8b) that is not present in the seismic model (Figure 1b). This seems to be counterintuitive because with the imposed plate motion history, one would expect that the shallow mantle structure be matched better. There are a number of possible reasons. 1) Seismic models have nonuniform resolution due to uneven path coverage (e.g., for the shallow mantle). This would suggest that more vigorous comparison techniques, such as those considering resolution operator [e.g., *Ritsema et al.*, 2007; *Bull et al.*, 2009] may be needed. 2) Our convection models ignore features such as 410 km and 670 km phase changes and continental keels at the shallow mantle, and postperoskite phase change at the large depths that may cause the reduced correlations at those depths. 3) A significant fraction of mantle materials at the relatively shallow mantle away from subduction zones may be derived from the deep mantle from more distant past and carry the thermal and structure history that is beyond what our convection models can resolve. Future studies should attempt to address these issues.

[59] Finally, we wish to point out that the models presented here did not consider possible composition-dependent viscosity [e.g., *McNamara and Zhong*, 2004a] and composition-dependent equation of state [e.g., *Tan and Gurnis*, 2005] for the dense components that may affect the morphology of the chemical piles above the CMB. We also ignored phase changes (e.g., at the 670 km depth and near the CMB) and did not consider purely thermal convection in our models [e.g., *Bull et al.*, 2009]. Our models can also be benefited from adding the plate reconstruction for the Pacific hemisphere at 140 Ma [*Muller et al.*, 2008]. While we do not think that these effects will significantly impact our main results including time evolution of the mantle structures, it is important to consider these effects in future studies.

5. Conclusions

[60] This work investigates time evolution of mantle structure in the African hemisphere and as well as on a global scale for the last supercontinent cycle since 450 Ma, using 3-D spherical mantle convection models that include time-dependent plate motion as the surface velocity boundary condition, depth- and temperature-dependent viscosity, and chemically dense piles above the CMB. Our results can be summarized as the follows.

[61] 1. We constructed a proxy model for global plate motion for the last 450 Myr. For the last 119 Myr, the global plate motion of *Lithgow-Bertelloni and Richards* [1998] was used. Before 119 Ma, the plate motion history for the African hemisphere was constrained by paleogeographic reconstruction of continents [*Scotese*, 2001], while divergent plate motions similar to that at 119 Ma are assumed for the Pacific hemisphere.

[62] 2. Using the proxy plate motion model as time-dependent boundary conditions, we showed that our convection models with relatively small buoyancy number (~0.5) reproduce well the basic features of the present-day mantle structure including the African and Pacific superplumes and chemical piles, and a predominantly degree 2 structure throughout the lower mantle.

[63] 3. Our models demonstrated that the mantle in the African hemisphere around the Pangea time is predominated by cold downwellings resulting from the convergence between Gondwana and Laurussia. The downwellings sweep aside the chemical piles from most of the African mantle. The present-day African superplume structure may not have been formed until ~100 Ma after Pangea formation, as a result of upwelling return flow in response to the circum-Pangea subduction.

[64] 4. The mantle in the Pacific hemisphere is predominated by a major upwelling system since the Pangea time, as a result of the assumed divergent plate motions there. Our calculations suggest that there cannot be significant plate convergence for the last ~300 Myr in the Pacific hemisphere. Our model results are consistent with the hypothesis by *Zhong et al.* [2007] for the time evolution of mantle structure in the African hemisphere and on a global scale in relation to supercontinent cycles, as well as the geodynamic history hypothesized for the Rodinia supercontinent cycle [*Li et al.*, 2004, 2008; *Li and Zhong*, 2009].

[65] **Acknowledgments.** We thank Adrian Lenardic and an anonymous reviewer for their careful reviews. This work is supported by the U.S. National Science Foundation, the David and Lucile Packard Foundation, and ARC Discovery Project grants (DP0770228). The CIG is thanked for distributing the software CitcomS that is used in this study. This is TIGeR publication 215.

References

Anderson, D. L. (1982), Hotspots, polar wander, Mesozoic convection and the geoid, *Nature*, *297*, 391–393, doi:10.1038/297391a0.

Becker, T. W., and L. Boschi (2002), A comparison of tomographic and geodynamic mantle models, *Geochem. Geophys. Geosyst.*, *3*(1), 1003, doi:10.1029/2001GC000168.

Bercovici, D., G. Schubert, and G. A. Glatzmaier (1989), Three-dimensional, spherical models of convection in the Earth's mantle, *Science*, *244*, 950–955, doi:10.1126/science.244.4907.950.

Boschi, L., T. W. Becker, and B. Steinberger (2007), Mantle plumes: Dynamic models and seismic images, *Geochem. Geophys. Geosyst.*, *8*, Q10006, doi:10.1029/2007GC001733.

Bull, A. L., A. K. McNamara, and J. Ritsema (2009), Synthetic tomography of plume clusters and thermochemical piles, *Earth Planet. Sci. Lett.*, *278*, 152–162, doi:10.1016/j.epsl.2008.11.018.

Bunge, H.-P., M. A. Richards, and J. R. Baumgardner (1996), The effect of depth-dependent viscosity on the planform of mantle convection, *Nature*, *379*, 436–438, doi:10.1038/379436a0.

Bunge, H.-P., M. A. Richards, C. Lithgow-Bertelloni, J. R. Baumgardner, S. Grand, and B. Romanowicz (1998), Time scales and heterogeneous structure in geodynamic Earth models, *Science*, *280*, 91–95, doi:10.1126/science.280.5360.91.

Burke, K., B. Steinberger, T. H. Torsvik, and M. A. Smethurst (2008), Plume generation zones at the margins of large low shear velocity provinces on the core-mantle boundary, *Earth Planet. Sci. Lett.*, *265*, 49–60, doi:10.1016/j.epsl.2007.09.042.

Chase, C. G., and D. R. Sprowl (1983), The modern geoid and ancient plate boundaries, *Earth Planet. Sci. Lett.*, *62*, 314–320, doi:10.1016/0012-821X(83)90002-X.

Collins, W. J. (2003), Slab pull, mantle convection, and Pangaean assembly and dispersal, *Earth Planet. Sci. Lett.*, *205*, 225–237, doi:10.1016/S0012-821X(02)01043-9.

Coltice, N., B. R. Phillips, H. Bertrand, Y. Ricard, and P. Rey (2007), Global warming of the mantle at the origin of flood basalts over supercontinents, *Geology*, *35*(5), 391–394, doi:10.1130/G23240A.1.

Condie, K. C. (2003), Incompatible element ratios in oceanic basalts and komatiites: Tracking deep mantle sources and continental growth rates with time, *Geochem. Geophys. Geosyst.*, *4*(1), 1005, doi:10.1029/2002GC000333.

Davaille, A. (1999), Simultaneous generation of hotspots and superswells by convection in a heterogeneous planetary mantle, *Nature*, *402*, 756–760, doi:10.1038/45461.

Davies, G. F. (1999), *Dynamic Earth: Plates, Plumes and Mantle Convection*, 470 pp., doi:10.1017/CBO9780511605802, Cambridge Univ. Press, Cambridge, U. K.

Davies, G. F., and F. Pribac (1993), Mesozoic seafloor subsidence and the Darwin Rise, past and present, in *The Mesozoic Pacific: Geology, Tectonics, and Volcanism*, *Geophys. Monogr. Ser.*, vol. 77, edited by S. Pringle et al., pp. 39–52, AGU, Washington, D. C.

Dziewonski, A. M. (1984), Mapping the lower mantle: Determination of lateral heterogeneity in P-velocity up to degree and order 6, *J. Geophys. Res.*, *89*, 5929–5952, doi:10.1029/JB089iB07p05929.

Engebretson, D. C., K. Kelley, H. Cashman, and M. R. Richards (1992), 180 million years of subduction, *GSA Today*, *2*, 93–96.

Foley, B., and T. W. Becker (2009), Generation of plate-like behavior and mantle heterogeneity from a spherical, visco-plastic convection model, *Geochem. Geophys. Geosyst.*, *10*, Q08001, doi:10.1029/2009GC002378.

Garnero, E. J., T. Lay, and A. McNamara (2007), Implications of lower mantle structural heterogeneity for existence and nature of whole mantle plumes, in *The Origin of Melting Anomalies: Plates, Plumes and Planetary Processes*, edited by G. R. Foulger and D. M. Jurdy, *Spec. Pap. Geol. Soc. Am.*, *430*, 79–101.

Gordon, R. G., and D. M. Jurdy (1986), Cenozoic global plate motions, *J. Geophys. Res.*, *91*, 12,389–12,406, doi:10.1029/JB091iB12p12389.

Grand, S. P., R. D. van der Hilst, and S. Widiyantoro (1997), Global seismic tomography: A snapshot of convection in the Earth, *GSA Today*, *7*(4), 1–7.

Grigné, C., S. Labrosse, and P. J. Tackley (2005), Convective heat transfer as a function of wavelength: Implications for the cooling of the Earth, *J. Geophys. Res.*, *110*, B03409, doi:10.1029/2004JB003376.

Gurnis, M. (1988), Large-scale mantle convection and the aggregation and dispersal of supercontinents, *Nature*, *332*, 695–699, doi:10.1038/332695a0.

Gurnis, M. (1993), Phanerozoic marine inundation of continents driven by dynamic topography above subducting slabs, *Nature*, *364*, 589–593, doi:10.1038/364589a0.

Hager, B. H., and R. J. O'Connell (1981), A simple global model of plate dynamics and mantle convection, *J. Geophys. Res.*, *86*, 4843–4867, doi:10.1029/JB086iB06p04843.

Hager, B. H., and M. A. Richards (1989), Long-wavelength variations in the Earth's geoid: Physical models and dynamic implications, *Philos. Trans. R. Soc. London, Ser. A*, *328*, 309–327, doi:10.1098/rsta.1989.0038.

Hager, B. H., R. W. Clayton, M. A. Richards, R. P. Comer, and A. M. Dziewonski (1985), Lower mantle heterogeneity, dynamic topography and the geoid, *Nature*, *313*, 541–545, doi:10.1038/313541a0.

He, Y., and L. X. Wen (2009), Structural features and shear-velocity structure of the "Pacific Anomaly", *J. Geophys. Res.*, *114*, B02309, doi:10.1029/2008JB005814.

Höink, T., and A. Lenardic (2008), Three-dimensional mantle convection simulations with a low-viscosity asthenosphere and the relationship between heat flow and the horizontal length scale of convection, *Geophys. Res. Lett.*, *35*, L10304, doi:10.1029/2008GL033854.

Jellinek, A. M., and M. Manga (2002), The influence of a chemical boundary layer on the fixity and lifetime of mantle plumes, *Nature*, *418*, 760–763, doi:10.1038/nature00979.

Kellogg, L. H., B. H. Hager, and R. van der Hilst (1999), Compositional stratification in the deep mantle, *Science*, *283*, 1881–1884, doi:10.1126/science.283.5409.1881.

King, S. D., J. P. Lowman, and C. W. Gable (2002), Episodic tectonic plate reorganizations driven by mantle convection, *Earth Planet. Sci. Lett.*, *203*, 83–91, doi:10.1016/S0012-821X(02)00852-X.

Larson, R. L. (1991), Latest pulse of Earth: Evidence for a Mid-Cretaceous super plume, *Geology*, *19*(6), 547–550, doi:10.1130/0091-7613(1991)019<0547:LPOEEF>2.3.CO;2.

Lawver, L. A., M. F. Coffin, L. M. Gahagan, D. A. Campbell, and J. Y. Royer (2004), PLATES 2004 atlas of plate reconstructions (750 Ma to present day), *PLATES Proj. Rep. 207*, Univ. of Tex. Inst. for Geophys., Austin.

Lay, T., and E. J. Garnero (2007), Reconciling the post-perovskite phase with seismological observations of lowermost mantle structure, in *Post-perovskite: The Last Mantle Phase Transition*, *Geophys. Monogr. Ser.*, vol. 174, edited by K. Hirose et al., pp. 129–154, AGU, Washington, D. C.

Lenardic, A., and W. M. Kaula (1994), Tectonic plates, D" thermal structure, and the nature of mantle plumes, *J. Geophys. Res.*, *99*, 15,697–15,708, doi:10.1029/94JB00466.

Lenardic, A., M. A. Richards, and F. H. Busse (2006), Depth-dependent rheology and the horizontal length scale of mantle convection, *J. Geophys. Res.*, *111*, B07404, doi:10.1029/2005JB003639.

Leng, W., and S. J. Zhong (2008), Viscous heating, adiabatic heating and energetic consistency in compressible mantle convection, *Geophys. J. Int.*, *173*, 693–702, doi:10.1111/j.1365-246X.2008.03745.x.

Li, X. H., Z. X. Li, W. X. Li, and Y. Wang (2006), Initiation of the Indosinian Orogeny in south China: Evidence for a Permian magmatic arc on Hainan Island, *J. Geol.*, *114*, 341–353, doi:10.1086/501222.

Li, Z. X., and X. H. Li (2007), Formation of the 1300-km-wide intracontinental orogen and postorogenic magmatic province in Mesozoic south China: A flat-slab subduction model, *Geology*, *35*(2), 179–182, doi:10.1130/G23193A.1.

Li, Z. X., and C. M. Powell (2001), An outline of the paleogeographic evolution of the Australasian region since the beginning of the Neoproterozoic, *Earth Sci. Rev.*, *53*, 237–277, doi:10.1016/S0012-8252(00)00021-0.

Li, Z. X., and S. J. Zhong (2009), Supercontinent-superplume coupling, true polar wander and plume mobility: Plate dominance in whole-mantle tectonics, *Phys. Earth Planet. Inter.*, *176*, 143–156, doi:10.1016/j.pepi.2009.05.004.

Li, Z. X., D. A. D. Evans, and S. Zhang (2004), A 90° spin on Rodinia: Possible causal links between the Neoproterozoic supercontinent, superplume, true polar wander and low-latitude glaciation, *Earth Planet. Sci. Lett.*, *220*, 409–421, doi:10.1016/S0012-821X(04)00064-0.

Li, Z. X., et al. (2008), Assembly, configuration, and break-up history of Rodinia: A synthesis, *Precambrian Res.*, *160*(1–2), 179–210, doi:10.1016/j.precamres.2007.04.021.

Lithgow-Bertelloni, C., and M. A. Richards (1998), Dynamics of Cenozoic and Mesozoic plate motions, *Rev. Geophys.*, *36*, 27–78, doi:10.1029/97RG02282.

Lithgow-Bertelloni, C., and P. G. Silver (1998), Dynamic topography, plate driving forces and the African Superswell, *Nature*, *395*, 269–272, doi:10.1038/26212.

Maruyama, S. (1994), Plume tectonics, *J. Geol. Soc. Jpn.*, *100*, 24–49.

Maruyama, S., Y. Isozaki, G. Kimura, and M. Terabayashi (1997), Paleogeographic maps of the Japanese islands: Plate tectonic synthesis from 750 Ma to the present, *Isl. Arc*, *6*, 121–142, doi:10.1111/j.1440-1738.1997.tb00043.x.

Maruyama, S., M. Santosh, and D. Zhao (2007), Superplume, supercontinent, and post-perovskite: Mantle dynamics and anti-plate tectonics on the core-mantle boundary, *Gondwana Res.*, *11*, 7–37, doi:10.1016/j.gr.2006.06.003.

Masters, G., G. Laske, H. Bolton, and A. Dziewonski (2000), The relative behavior of shear velocity, bulk sound speed, and compressional velocity in the mantle: Implications for chemical and thermal structure, in *Earth's Deep Interior: Mineral Physics and Tomography From the Atomic to the Global Scale*, *Geophys. Monogr. Ser.*, vol. 117, edited by S. Karato et al., pp. 63–87, AGU, Washington, D. C.

McNamara, A. K., and S. J. Zhong (2004a), Thermochemical structures within a spherical mantle: Superplumes or piles?, *J. Geophys. Res.*, *109*, B07402, doi:10.1029/2003JB002847.

McNamara, A. K., and S. J. Zhong (2004b), The influence of thermochemical convection on the fixity of mantle plumes, *Earth Planet. Sci. Lett.*, *222*, 485–500, doi:10.1016/j.epsl.2004.03.008.

McNamara, A. K., and S. J. Zhong (2005), Thermochemical structures beneath Africa and the Pacific Ocean, *Nature*, *437*, 1136–1139, doi:10.1038/nature04066.

Moresi, L. N., and M. Gurnis (1996), Constraints on the lateral strength of slabs from three-dimensional dynamic flow models, *Earth Planet. Sci. Lett.*, *138*, 15–28, doi:10.1016/0012-821X(95)00221-W.

Muller, R. D., M. Sdrolias, C. Gaina, B. Steinberger, and C. Heine (2008), Long-term sea-level fluctuations driven by ocean basin dynamics, *Science*, *319*, 1357–1362, doi:10.1126/science.1151540.

Nance, R. D., T. R. Worsley, and J. B. Moody (1988), The supercontinent cycle, *Sci. Am.*, *259*, 72–79, doi:10.1038/scientificamerican0788-72.

Ni, S., E. Tan, M. Gurnis, and D. V. Helmberger (2002), Sharp sides to the African superplume, *Science*, *296*, 1850–1852, doi:10.1126/science.1070698.

Ni, S., D. V. Helmberger, and J. Tromp (2005), Three-dimensional structure of the Africa superplume from waveform modeling, *Geophys. J. Int.*, *161*(2), 283–294, doi:10.1111/j.1365-246X.2005.02508.x.

Nyblade, A. A., and S. W. Robinson (1994), The African superswell, *Geophys. Res. Lett.*, *21*, 765–768, doi:10.1029/94GL00631.

O'Neill, C., A. Lenardic, A. M. Jellinek, and L. Moresi (2009), Influence of supercontinents on deep mantle flow, *Gondwana Res.*, *15*, 276–287, doi:10.1016/j.gr.2008.11.005.

Phillips, B. R., and P. H. Bunge (2005), Heterogeneity and time dependence in 3D spherical mantle convection models with continental drift, *Earth Planet. Sci. Lett.*, *233*, 121–135, doi:10.1016/j.epsl.2005.01.041.

Phillips, B. R., and P. H. Bunge (2007), Supercontinent cycles disrupted by strong mantle plumes, *Geology*, *35*, 847–850, doi:10.1130/G23686A.1.

Pollack, H. N., S. J. Hurter, and J. R. Johnson (1993), Heat loss from the Earth's interior: Analysis of the global data set, *Rev. Geophys.*, *31*(3), 267–280, doi:10.1029/93RG01249.

Prokoph, A., R. E. Ernst, and K. L. Buchan (2004), Time-series analysis of large igneous provinces: 3500 Ma to present, *J. Geol.*, *112*(1), 1–22, doi:10.1086/379689.

Reeves, C., and M. de Wit (2000), Making ends meet in Gondwana: Retracing the transforms of the Indian Ocean and reconnecting continental shear zones, *Terra Nova*, *12*, 272–280, doi:10.1046/j.1365-3121.2000.00309.x.

Ricard, Y., M. A. Richards, C. Lithgow-Bertelloni, and Y. Lestunff (1993), A geodynamic model of mantle mass heterogeneities, *J. Geophys. Res.*, *98*, 21,895–21,909, doi:10.1029/93JB02216.

Ritsema, J., H. J. van Heijst, and J. H. Woodhouse (1999), Complex shear wave velocity structure imaged beneath Africa and Iceland, *Science*, *286*, 1925–1928, doi:10.1126/science.286.5446.1925.

Ritsema, J., A. K. McNamara, and A. L. Bull (2007), Tomographic filtering of geodynamic models: Implications for model interpretation and large-scale mantle structure, *J. Geophys. Res.*, *112*, B01303, doi:10.1029/2006JB004566.

Romanowicz, B., and Y. C. Gung (2002), Superplumes from the core-mantle boundary to the lithosphere: Implications for heat flux, *Science*, *296*, 513–516, doi:10.1126/science.1069404.

Scotese, C. R. (1990), Atlas of Phanerozoic plate tectonic reconstructions, *Tech. Rep. 10-90-1*, PALEOMAP Proj., Dep. of Geol., Univ. of Tex. at Arlington.

Scotese, C. R. (1997), *Continental Drift*, 7th ed., 79 pp., PALEOMAP Proj., Arlington, Tex.

Scotese, C. R. (2001), Atlas of Earth history, *PALEOMAP Progress Rep. 90-0497*, Dep. of Geol., Univ. of Tex. at Arlington, Arlington.

Smith, A. G., A. M. Hurley, and J. C. Briden (1981), *Phanerozoic Paleocontinental World Maps*, 102 pp., Cambridge Univ. Press, New York.

Steinberger, B., and M. Antretter (2006), Conduit diameter and buoyant rising speed of mantle plumes: Implications for the motion of hot spots and shape of plume conduits, *Geochem. Geophys. Geosyst.*, *7*, Q11018, doi:10.1029/2006GC001409.

Steinberger, B., and R. J. O'Connell (1998), Advection of plumes in mantle flow: Implications for hotspot motion, mantle viscosity and plume distribution, *Geophys. J. Int.*, *132*, 412–434, doi:10.1046/j.1365-246x.1998.00447.x.

Su, W. J., and A. M. Dziewonski (1997), Simultaneous inversion for 3-D variations in shear and bulk velocity in the mantle, *Phys. Earth Planet. Inter.*, *100*, 135–156, doi:10.1016/S0031-9201(96)03236-0.

Tackley, P. J. (1998), Three-dimensional simulations of mantle convection with a thermochemical CMB boundary layer: D"? in *The Core-Mantle Boundary Region*, *Geodyn. Ser.*, vol. 28, edited by M. Gurnis et al., pp. 231–253, AGU, Washington, D. C.

Tackley, P. J., D. J. Stevenson, G. A. Glatzmaier, and G. Schubert (1993), Effects of an endothermic phase transition at 670 km depth in a spherical model of convection in the Earth's mantle, *Nature*, *361*(6414), 699–704, doi:10.1038/361699a0.

Tan, E., and M. Gurnis (2005), Metastable superplumes and mantle compressibility, *Geophys. Res. Lett.*, *32*(20), L20307, doi:10.1029/2005GL024190.

Thorne, M., E. J. Garnero, and S. Grand (2004), Geographic correlation between hot spots and deep mantle lateral shear-wave velocity gradients, *Phys. Earth Planet. Inter.*, *146*, 47–63, doi:10.1016/j.pepi.2003.09.026.

Torsvik, T. H., J. G. Meert, R. Van der Voo, W. S. McKerrow, M. D. Brasier, B. A. Sturt, and H. J. Walderhaug (1996), Continental break-up and collision in the Neoproterozoic and Paleozoic—A tale of Baltica and Laurentia, *Earth Sci. Rev.*, *40*, 229–258, doi:10.1016/0012-8252(96)00008-6.

Torsvik, T. H., M. A. Smethurst, K. Burke, and B. Steinberger (2006), Large igneous provinces generated from the margins of the large low-velocity provinces in the deep mantle, *Geophys. J. Int.*, *167*, 1447–1460, doi:10.1111/j.1365-246X.2006.03158.x.

Torsvik, T. H., B. Steinberger, L. R. M. Cocks, and K. Burke (2008a), Longitude: Linking Earth's ancient surface to its deep interior, *Earth Planet. Sci. Lett.*, *276*, 273–282, doi:10.1016/j.epsl.2008.09.026.

Torsvik, T. H., R. D. Muller, R. Van der Voo, B. Steinberger, and C. Gaina (2008b), Global plate motion frames: Toward a unified model, *Rev. Geophys.*, *46*, RG3004, doi:10.1029/2007RG000227.

Torsvik, T. H., M. A. Smethurst, K. Burke, and B. Steinberger (2008c), Long term stability in deep mantle structure: Evidence from the ~300 Ma Skagerrak-Centered Large Igneous Province (the SCLIP), *Earth Planet. Sci. Lett.*, *267*(3–4), 444–452, doi:10.1016/j.epsl.2007.12.004.

van der Hilst, R. D. (1997), Evidence for deep mantle circulation from global tomography, *Nature*, *386*, 578–584, doi:10.1038/386578a0.

van der Hilst, R. D., M. V. de Hoop, P. Wang, S.-H. Shim, P. Ma, and L. Tenorio (2007), Seismostratigraphy and thermal structure of Earth's core-mantle boundary region, *Science*, *315*, 1813–1817, doi:10.1126/science.1137867.

van Heck, H., and P. J. Tackley (2008), Planforms of self-consistently generated plate tectonics in 3-D spherical geometry, *Geophys. Res. Lett.*, *35*, L19312, doi:10.1029/2008GL035190.

Veevers, J. J. (2004), Gondwanaland from 650–500 Ma assembly through 320 Ma merge in Pangea to 185–100 Ma break-up: Supercontinental tec-

tonics via stratigraphy and radiometric dating, *Earth Sci. Rev.*, *68*, 1–132, doi:10.1016/j.earscirev.2004.05.002.

Wang, Y., and L. X. Wen (2004), Mapping the geometry and geographic distribution of a very-low velocity province at the base of the Earth's mantle, *J. Geophys. Res.*, *109*, B10305, doi:10.1029/2003JB002674.

Wen, L. X., P. Silver, D. James, and R. Kuehnel (2001), Seismic evidence for a thermo-chemical boundary at the base of the Earth's mantle, *Earth Planet. Sci. Lett.*, *189*, 141–153, doi:10.1016/S0012-821X(01)00365-X.

Zhang, N., S. J. Zhong, and A. K. McNamara (2009), Supercontinent formation from stochastic collision and mantle convection models, *Gondwana Res.*, *15*, 267–275, doi:10.1016/j.gr.2008.10.002.

Zhong, S. J. (2006), Constraints on thermochemical convection of the mantle from plume heat flux, plume excess temperature and upper mantle temperature, *J. Geophys. Res.*, *111*, B04409, doi:10.1029/2005JB003972.

Zhong, S. J., and M. Gurnis (1993), Dynamic feedback between a continent-like raft and thermal convection, *J. Geophys. Res.*, *98*, 12,219–12,232, doi:10.1029/93JB00193.

Zhong, S. J., and M. Gurnis (1994), The role of plates and temperature-dependent viscosity in phase change dynamics, *J. Geophys. Res.*, *99*, 15,903–15,917, doi:10.1029/94JB00545.

Zhong, S. J., M. T. Zuber, L. N. Moresi, and M. Gurnis (2000), Role of temperature-dependent viscosity and surface plates in spherical shell models of mantle convection, *J. Geophys. Res.*, *105*, 11,063–11,082, doi:10.1029/2000JB900003.

Zhong, S. J., N. Zhang, Z. X. Li, and J. H. Roberts (2007), Supercontinent cycles, true polar wander, and very long wavelength mantle convection, *Earth Planet. Sci. Lett.*, *261*, 551–564, doi:10.1016/j.epsl.2007.07.049.

W. Leng, N. Zhang, and S. Zhong, Department of Physics, University of Colorado, 390 UCB, Boulder, CO 80309, USA. (nan.zhang@colorado.edu)

Z.-X. Li, Department of Applied Geology, Curtin University of Technology, GPO Box U1987, Perth, WA 6845, Australia.